

Geomorphometric characterization and sediment connectivity of the middle Brahmaputra River basin

B. M. Refat Faisal[1, 2]

Corresponding author

Email: refatfaisal@ees.hokudai.ac.jp

Yuichi S. Hayakawa[3]

Email: hayakawa@ees.hokudai.ac.jp

(Institutional addresses)

[1] Graduate School of Environmental Science, Hokkaido University, Sapporo, Hokkaido 060-0810, Japan.

[2] Bangladesh Space Research and Remote Sensing Organization (SPARRSO), Agargaon, Sher-e-Bangla Nagar, Dhaka-1207, Bangladesh.

[3] Faculty of Environmental Earth Science, Hokkaido University, Sapporo, Hokkaido 060-0810, Japan.

Abstract

Knowledge of geomorphic characteristics and sediment connectivity is critical in understanding basin-scale surface processes that include steep mountainous and flat lowlands, particularly if the mid-basin and downstream areas are densely populated and disaster-prone. However, the lack of fluvial and sediment connectivity studies in downstream portions of large rivers of South Asia (particularly Bangladesh), where upper basin morphodynamics, hydrology, and sediment flux highly influence the repeated sediment disasters, limits our understanding of the large-scale fluvial geomorphic processes and basin-scale sustainable river management. Therefore, this article attempts to characterize the morphometric and topographic features along with the spatial sediment connectivity pattern of the middle Brahmaputra River basin (Teesta, Torsa, and Manas basins) covering ~75,000 km^2 that influences the hydro-geomorphic response of the deltaic landscape of lowland Bangladesh. This work considers a set of morphometric and topographic parameters including the stream network, longitudinal profiles, stream power index (SPI), and topographic wetness index (TWI) for geomorphometric characterization. The linkage between the sediment sources to downstream areas also has been evaluated with the sediment connectivity (IC) index to understand better the sediment dynamics of the middle Brahmaputra River basin, draining towards lowland Bangladesh from the basin's upstream countries of India and Bhutan. The result of this study demonstrates a highly potential hydro-geomorphic response of the downstream areas attributed to steep topography, steep channel longitudinal profiles, high rainfall, and high sediment connectivity in upstream regions. However, the low topography, presence of anthropogenic stressors, almost flat longitudinal channel profiles with limited change in elevation, and lowered sediment connectivity potential in the mid-to-downstream areas depicts sensitivity to the depositional processes therein, impacting the basin-scale geomorphic connectivity from the upstream to the

downstream region. These results will be the basic information for exploring the large-scale hydro-geomorphic response and structural sediment dynamics to understand the complex geomorphological processes in the South Asia region, where the fluvial sedimentation process is not fully understood with limited accessibility for field-based investigations.

Keywords: Brahmaputra, Himalayan upstream, NASA–DEM, Geomorphometry, Terrain analysis, sediment connectivity.

1. Introduction

Morphometry is the mathematical quantification of basin physiography (Clarke, 1966; Swarnkar et al., 2020; Oyedotun, 2020). It is crucial for characterizing geomorphological processes and understanding the evolutionary history of any basin (Sharma and Sarma, 2013). The morphological characteristics can be understood more clearly through linear, areal, and relief morphometric parameters (Mahala, 2020). Morphometric properties such as catchment area, stream network density, relief, terrain roughness, slope, and geology greatly influence the geomorphological changes and sediment connectivity in a basin (Fryirs et al., 2007; Cavalli and Marchi, 2008; Oguchi et al., 2013; Cavalli et al., 2013). Geomorphological studies also play an essential role in understanding the river system's longitudinal and lateral linkages (Sinha et al., 2005; Sinha et al., 2013). Moreover, morphometric analysis is crucial for sustainable watershed management, especially for upstream fluvial process-dominated downstream countries like Bangladesh, where integrated basin information is scarce (Sujatha et al., 2014; Rahmati et al., 2019).

Mountainous topography significantly impacts the spatial variation of hydrological conditions, including the spatial distribution of soil moisture and groundwater flow (Rahmati et al., 2019; Li et al., 2021). Notably, research of debris flow and sediment dynamics uses topographic factors like the topographic wetness index (TWI), the stream power index (SPI), the sediment transport index (STI), and the slope-length (LS) factor (De Reu et al., 2013; Rahmati et al., 2019). The use of digital elevation models (DEMs) to derive these topographic variables is faster, less subjective, and the obtained measurements are more reproducible than conventional techniques (Iqbal et al., 2005). In addition, using topographic indices for the large area that undergoes limited hydrological process monitoring, such as rainfall, runoff, and sediment yield, can provide helpful information for better watershed management. Moreover, the topographic factors correlate with drainage basin morphometry and impact the integrated watershed management (Sujatha et al., 2014).

Sediment connectivity is the degree to which a geomorphic system facilitates the transfer of sediment through its components such as hillslopes, channel networks, and valley bottoms (Fryirs and Brierley, 2013; Heckmann et al., 2018). The degree of connectivity between hillslopes and the channel and the transfer of water and sediment within the channel largely depends on the morphological diversity, where connectivity decreases with increasing landscape morphological complexity (Baartman et al., 2013). The connectivity processes also vary in space and time and can be modified by anthropogenic changes (drainage system changes, river engineering structures, land use, etc.) in the landscapes (Brierley et al., 2006; Jain and Tandon, 2010; Tarolli and Sofia, 2016; Llena et al., 2019). Measuring structural sediment connectivity is fundamental to representing the spatial configurations of the linkages among the components, which can be measured indirectly by using a geomorphic connectivity index instead of measuring connectivity in the field (Heckmann et al., 2018). Among several approaches to evaluating sediment connectivity, the use of geomorphometric indices (sediment connectivity index) make it possible to detect the areas that are prone to sediment transfer and the degree of sediment linkage through landscape units (Borselli et al., 2008; Cavalli et al., 2013; Persichillo et al., 2018; Zanandrea et al., 2019; Turley et al., 2021). This sediment connectivity index (IC), developed by Borselli et al. (2008) and then refined by Cavalli et al. (2013), is widely used and considered an effective means to quantitatively evaluate the transfer of sediments from hillslopes to downstream. This index helps identify the preferential sediment pathways and prioritize sediment source areas (Heckmann et al., 2018).

Although the downstream area of the Brahmaputra basin in South Asia is densely populated and highly prone to repeated sediment disasters, the research on hydro-geomorphic systems of the basin, considering the sediment linkage from upstream to downstream sink areas, has been limited (Faisal and Hayakawa, 2022). The sediment connectivity approach is essential in developing countries where the spatial data is often scarce and not easily accessible for field observation (Najafi et al., 2021). Moreover, there are few possibilities to model spatial patterns of sediment delivery and identify sediment source and sink areas because of the lack of effective and comprehensive strategies for basin-scale sediment management in the transboundary Brahmaputra River, which is shared by China, India, Bhutan, and Bangladesh in South Asia. Furthermore, understanding sediment connectivity informs us of sediment movement from source to sink in a catchment, which determines the long-term behavior of sediment flux and the aggradation or degradation patterns that are manifest as a change in the landforms (Bracken et al., 2015; Poeppl et al., 2017; Najafi et al., 2021). Therefore, understanding geomorphic characteristics and sediment connectivity patterns in the upstream-dominated Brahmaputra River basin is essential in sustainable water resources management and land use planning of downstream countries affected by high erosion and sediment delivery rates from its upstream regions.

This work focuses on the transboundary Himalayan-fed middle Brahmaputra River, distinguished by highly variable seasonal flows, significant sediment discharge, and diverse morphological patterns (Subramanian and Ramanathan, 1996; Islam et al., 1999; Singh et al., 2004; Mahanta et al., 2014). Despite the enormity and geomorphic diversity of the Brahmaputra River, comparatively little attention has been paid by national and international researchers during the past few decades compared to the Ganges River system (Coleman, 1969; Goswami, 1985; Umitsu, 1987; Sinha and Friend, 1994; Subramanian and Ramanathan, 1996; Allison et al., 1998; Islam et al., 1999; Kale, 2005; Sinha et al., 2005; Takagi et al., 2007; Goodbred et al., 2014; Brammer, 2014; Sarker et al., 2014; Dewan et al., 2017; Bandyopadhyay et al., 2021). Furthermore, the review of geomorphological processes and their connectivity in hillslope, fluvial, and coastal areas of the downstream portions of the Ganges–Brahmaputra depicts that fluvial-geomorphic research in the deltaic landscape of Bangladesh is explored at a small-scale (country scale) (Faisal and Hayakawa, 2022). These small-scale studies are insufficient to understand large-scale landscape processes (Lane and Richards, 1997; Jain et al., 2012). Notably, the upper basin morphodynamics, hydrology, and sediment flux of the Brahmaputra River system influence the fluvial sediment dynamics of the downstream Bangladesh (Subramanian and Ramanathan, 1996; Singh, 2007; Faisal and Hayakawa, 2022). Furthermore, the hydrological processes in the upper part of a river basin may directly influence downstream areas from a few to many hundreds of kilometers away (Nepal et al., 2014). Moreover, understanding upstream-dominated processes or events or sediment transport dynamics that shape the particular landform development of downstream areas is critical in geomorphic science (Whipple and Tucker, 1999; Stark and Stark, 2001).

A research gap exists in the geomorphological investigation of the middle Brahmaputra River basin (Faisal and Hayakawa, 2022), but the geomorphic characterization and sediment connectivity at a basin-wide scale would increase our knowledge about this river system and its downstream consequences. To fill the gap, the present research intends to analyze the morphometric characteristics, topographic features, and sediment connectivity along the right bank of the middle Brahmaputra River (Teesta, Torsa, and Manas) that are assumed to have a potential hydro-geomorphic response to the downstream area (Fig. 1). This article aimed to assess the geomorphic characteristics to compare sediment connectivity parameters (IC, SPI, etc.) between upland and lowland systems on the Brahmaputra River basins. The results from this study would be helpful in better understanding the basin-scale fluvial-geomorphic processes and may provide baseline information for further research.

2. Study area

2.1 Area of interest (AOI)

The Brahmaputra River (580,000 km^2 drainage area) is known as Yarlung/Tsang Po in China (Tibet), Siang/Dihang River in Arunachal Pradesh (India), Lohit/Dilao in Assam (India), and Jamuna in Bangladesh, characterized by marked variability in its substantial discharge and a considerable amount of sediment volume (~721 million t/yr) (Goswami, 1985; Sharma et al., 2012; Faisal and Hayakawa, 2022). The geology of the Brahmaputra basin is comprised of the Higher Himalaya (schists, gneisses, marbles with amphiboles, Migmatites, and Miocene leucogranites), the Lesser Himalaya (schists, quartzites, graphitic schists, and limestone) and the Siwaliks formation (Singh and France-Lanord, 2002; Singh, 2007; Goodbred et al., 2014). The northern tributaries joining the Brahmaputra in Assam largely drain metamorphic rocks of the Higher Himalayas in Bhutan and Sikkim (Garzanti et al., 2004). The low-grade sedimentary rocks of the Lesser Himalaya outcrop locally along the Assam Valley tributaries in the Brahmaputra catchment (Richards et al., 2006; Goodbred et al., 2014). The Assam and Bangladesh plains carry the Brahmaputra's fluvial sediments consisting of alluvial features such as natural levees, point bars, oxbow lakes, and channel bars (Goswami, 1998; Singh, 2007).

Most of the Brahmaputra's sediment load is derived from its high Himalayan portion and many landslides in this region, transferring sediment downstream and causing large floods with substantial flood deposits (Wasson, 2003; Rajbanshi et al., 2022). Rainfall during the southwest monsoon (June–September) is a significant source of water and contributes to the annual discharge of the Brahmaputra. However, Himalayan meltwater and groundwater contributions are crucial during summer (Singh, 2007). In this study, we want to emphasize the mountainous northern (right bank) tributaries of the middle Brahmaputra River (Fig. 1) considering its dynamic characteristics (i.e., high flow and sediment contribution, extensive channel modification, steeper channel gradient, and flashy nature) compared to the south bank tributaries (Sharma et al., 2012; Pangare et al., 2021). For example, the Teesta, Torsa, and Manas contribute significantly to the discharge of the main Brahmaputra (Sarma, 2004; Saha and Bhattacharya, 2021; Pangare et al., 2021) and may influence the sediment flux as well as sediment transfer at its entire catchment.

Therefore, north bank tributaries joining the mainstream Brahmaputra River channel adjacent and upstream to the Bangladesh border, namely Teesta, Torsa, and Manas basins, have been selected for the present study. The selected basins fall within the Pandu to Goalundo reach (Sarma, 2004). After rising from the northern Himalayan, the Teesta traverses 309 km to join the Jamuna below Rangpur town in Bangladesh (Sarma, 2004). The Torsa travels about 145 km through the Chumbi valley of Bhutan before entering India near Ramgati, called Amo Chu. The Torsa travels a distance of 100 km through North Bengal, and after flowing past Balampur, it joins the Jamuna 15 km downstream from the last Indian tributary, the Gangadhar (Saha and Bhattacharya, 2019, 2021). The Manas originates from the northern slope of Mount Kula Kangri in Tibet and flows 140 km through Bhutan; then, it bifurcates near the Indian border and travels through the Assam valley before meeting the Brahmaputra. The area of interest for this study is about 75,000 km^2, which connects different parts of India and Bhutan and flows through the main Brahmaputra channel to downstream Bangladesh farther south (Rasul, 2015; Ray et al., 2015). Table 1 identifies the significant characteristics of the selected basins.

Table 1. Major characteristics of basins under this study

Characteristics	Basin		
	(1) Teesta	(2) Torsa	(3) Manas
Basin area (km^2)	17,639	23,680	33,102
Mean elevation (m)	3173	2479	3298
Annual average rainfall (mm) (2010-2019)	2408	1763	1200
Average annual yield in Million Cubic Meter (MCM)	21,413	14,980	2925
Major land-cover	Trees (40.68%), Crops (17.46%), Shrubs (13.27%), Built up (11.09%), Bare ground (8.25%), Water (2.38%)	Trees (54.77%), Shrubs (19.44%), Crops (8.44%), Built up (5.08%), Bare ground (5.81%), water (1.31%)	Trees (45.04%), Shrubs (25.76%), Bare ground (14.34%), Crops (5.50%), Built up (3.09%), water (1.37%)

Note: Based on Brahmaputra Board, 1995; TRMM, 2011; Mahanta et al., 2014; NASA JPL, 2020; Karra et al., 2021; Pangare et al., 2021

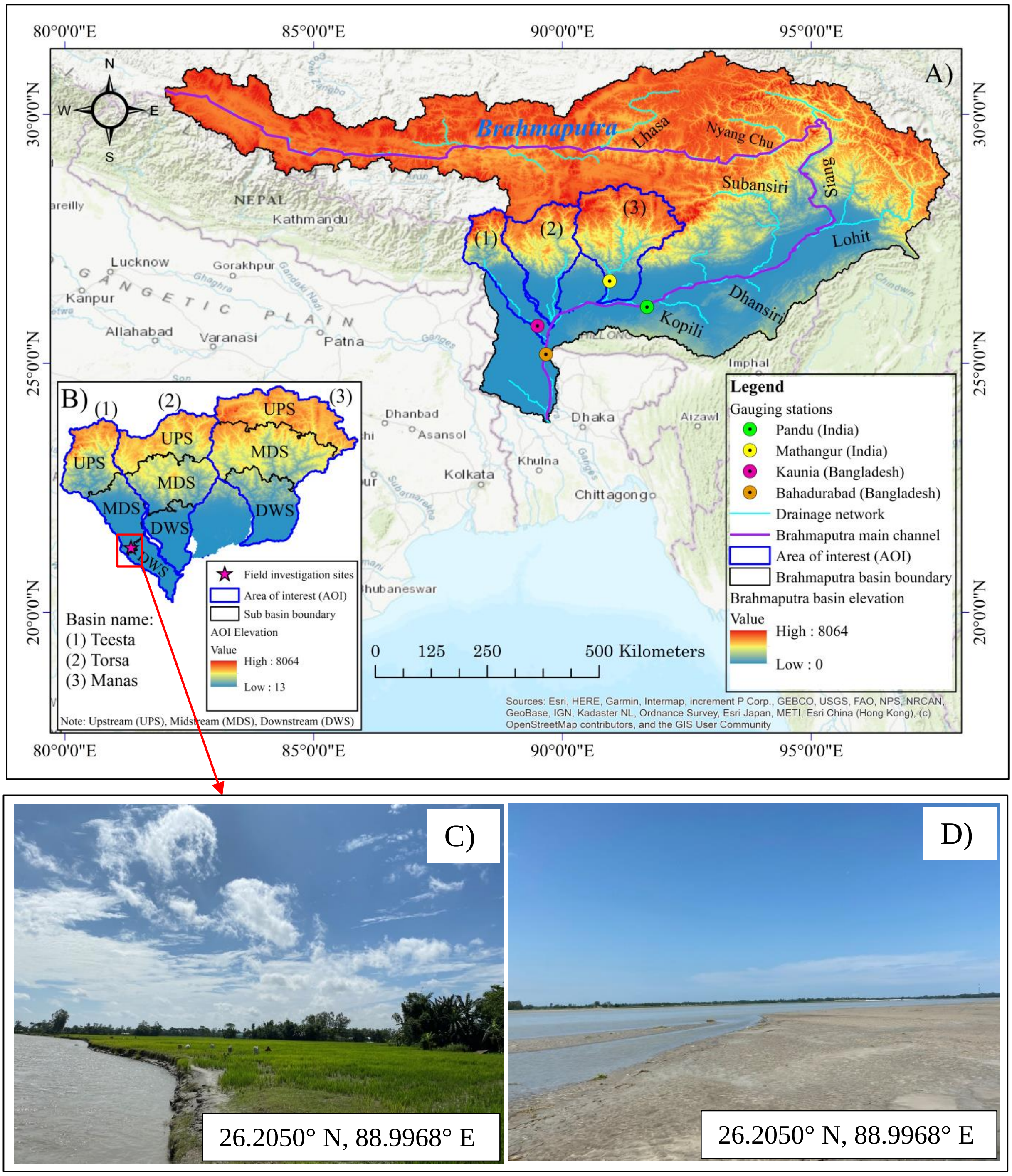

Fig. 1. A) Overview of Brahmaputra River basin with background topography showing the flow path connecting the upstream region to downstream and surrounding areas, B) the area of interest; upstream (UPS), midstream (MDS), and downstream (DWS), C-D) field photos were taken by the authors on 20 Aug 2022 from the field investigation site (Indicated in Fig. 1B), Teesta River (Brahmaputra's tributary) in northern Bangladesh; where C) and D) respectively show the erosion along the bank and sedimentation within the channel.

2.2 Meteorological conditions

The entire Brahmaputra basin, excluding the Tibetan portion, falls within the Southeast Asian monsoon regime, highly influenced by extreme monsoon rainfall with a mean annual rainfall of 2300 mm (Mahanta et al., 2014). The monsoon rain (June to September) accounts for 60-70% of the yearly rainfall in the entire Brahmaputra basin, while the pre-monsoon season (March to May) produces only 20-25% of the annual rainfall (Mahanta et al., 2014). The large concentrated rainfall pattern in the monsoon season may increase the basin discharge, generating a high sediment yield and dynamics (Mahanta et al., 2014; Pangare et al., 2021). Hence, the tropical rainfall measuring missions (TRMM) data from (2010-2019) have been analyzed to observe the rainfall pattern over the studied basins. The time series analysis of rainfall data also suggests strong monsoonal influence (June to September) with an average annual rainfall of 1200 mm to 2408 mm along these basins (Fig. 2).

In addition, the enormous and variable flows distinguish the hydrological regimes, where about 70-80% of the total Brahmaputra discharge is from the southwest monsoon (Singh, 2007). The hydrographs of available average annual discharge along the studied basins indicates monsoonal (June to September/October) flow dominancy (Supplementary Fig. S1). For example, at Bahadurabad (Bangladesh) gauging station (where the Teesta at downstream Bangladesh joins the Brahmaputra), the average monsoon flow is 35,712 m^3/s. In contrast, during the non-monsoonal season (January–April), the average flow is 5186 m^3/s (Rahaman and Varis, 2009). Therefore, the mainstream and the tributaries of the Brahmaputra spill over their banks, causing devastating floods in the Assam plains and Bangladesh annually during the southwest monsoon (Kale, 2003). The similar scenario of rainfall patterns and annual discharge at different parts of the Brahmaputra basin were mentioned in previous studies (Mahanta et al., 2014; Rao et al., 2020; Pangare et al., 2021).

The rainfall and discharge patterns have been considered here to discuss the effects of hydro-meteorological conditions on these basins' characteristics and sediment dynamics.

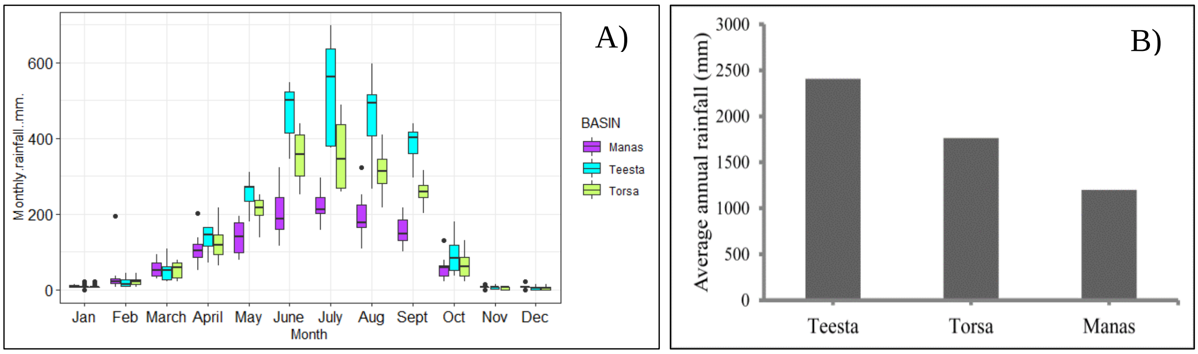

Fig. 2. Inter-basin A) monthly rainfall cycle and B) average annual rainfall variations throughout 2010-2019.

3. Data and methods

3.1 Geospatial data

Table 2 provides a summary of the dataset used in this study. Freely accessible NASA-DEM_HGT (30 m and void-filled), created by the NASA-MEaSUREs program (publicly released in February 2020), have been downloaded from NASA-LPDAAC (Land Processes Distributed Active Archive Center) (NASA JPL, 2020; Buckley et al., 2020). This NASA-DEM is reprocessed from the radar-based SRTM (Shuttle Radar Topographic Mission) with many improvements to its quality, notably void reduction and artifacts removal using auxiliary data from various datasets such as ASTER GDEM, PRISM (Panchromatic Remote-sensing Instrument for Stereo Mapping), GLAS (Geoscience Laser Altimeter System), and ICESat (Ice, Cloud, and Land Elevation Satellite) in processing techniques (Crippen et al., 2016, Buckley et al., 2020; Oguchi et al., 2022; Tran et al., 2023). The vertical accuracy of NASA-DEM has been revealed as 5.3 m (USA) (Buckley et al., 2020), 6.39 m (Estonian) (Uuemaa et al., 2020), 6.59 m (China) (Li et al., 2022), and 12.08 m (New Zealand) (Uuemaa et al., 2020). Moreover, the NASA Jet propulsion laboratory (creators of the dataset) claims that the radar does an excellent job in penetrating the vegetation canopy, so the digital terrain model (DTM) bias is not significant (Franks et al., 2020). Since NASA-DEM is relatively new, few articles have been published in the relevant fields of study and performed well compared to other freely available global DEM datasets, e.g., ASTER, AW3D30, MERIT, SRTM, and TanDEM-X (Franks et al., 2020; Uuemaa et al., 2020; Li et al., 2020; Tran et al., 2023).

Here, space borne rainfall data from TRMM-3B43, which was a joint mission between NASA and the Japan aerospace exploration agency (JAXA), have been used to extract the meteorological information (rainfall) from 2010 to 2019 over the area of interest (TRMM, 2011). The TRMM system uses precipitation RADAR, microwave imager, and visible infrared scanner merged with station data to estimate rainfall (Huffman et al., 2007; NASA, 2017). Furthermore, freely accessible Brahmaputra River discharge data from three gauging stations (shown in Fig. 1) along the present study area have been accessed from the global runoff datacenter (GRDC) website (GRDC, 2021). Unfortunately, these discharge datasets are widely spaced with a large data gap (7 to 10 yr) and historic (time series data collection ends around 1990) (Goswami, 1985; Islam et al., 1999; Sarma, 2005). The available time series insitu discharge datasets (Table 2) are used to discuss the large-scale flow dynamics and sediment connectivity patterns along these basins. In addition, the most comprehensive and updated instrumental discharge data of Bahadurabad (Bangladesh) gauging station over the last six decades (1956-2011) have been collected from Rao et al. (2020) for this study**.** However, the combination of NASA-DEM, TRMM rainfall, and river discharge data at gauging stations provides a new dimension in the investigation of hydro-geomorphological characteristics of the study area.

The global land-use/land-cover (LULC) 2020 maps derived from European space agency (ESA) Sentinel-2 imageries at 10 m resolution released by Environmental System

Research Institute Inc. (ESRI) under creative commons BY-4.0 license in July 2021 have been used in this study (Karra et al., 2021). Furthermore, in association with IUCN (International Union for Conservation of Nature and Natural Resources) and collaborative research between India and Bangladesh, the physical assessment report of Brahmaputra basin-2014 provides previously unavailable annual sediment yield data for future research in the under-investigated Brahmaputra basin (Brahmaputra Board, 1995; Mahanta et al., 2014; Pangare et al., 2021). Our study intends to use this yield estimation data collected from Brahmaputra Board (India) and an extensive joint field investigation between India and Bangladesh. The ground-based sediment yield data collection and availability are highly appreciated because the field data collection in the transboundary Brahmaputra River is somewhat risky with limited accessibility, hindering a systematic field-based investigation.

We also used a global polygon for terrain classification data released in June 2022 by the geospatial information authority of Japan (GSI) as a proxy for the topographic applications (Iwahashi and Yamazaki, 2022). The geometric signatures of terrain polygons such as lnSLOPE, lnHAND (Height Above the Nearest Drainage), and Texture (density of pits and peaks) that quantitatively classify the topography help obtain an overview of the ground efficiently in a wide area (Iwahashi et al., 2021).

Table 2. Data used in the present study

Input data	Data source	Specifications	Reference
NASA-DEM	NASA-MEaSUREs (https://earthexplorer.usgs.gov/)	30 m spatial resolution and released in 2020.	NASA JPL, 2020; Buckley et al., 2020
Annual average rainfall	TRMM (https://disc2.gesdisc.eosdis.nasa.gov/opendap/)	TRMM_3B43 version 7; 0.25° by 0.25° spatial resolution over the period of 2010-2019.	TRMM, 2011
Land-use and land-cover	ESRI 2021 (https://livingatlas.arcgis.com/landcover/)	ESA Sentinel-2 (10 m) released in July 2021.	Karra et al., 2021
Average annual yield (MCM)	IUCN 2014 (https://www.iucn.org/content/physical-assessment-brahmaputra-river)	IUCN report on physical assessment of the Brahmaputra river: A Bangladesh-India Initiative.	Mahanta et al., 2014
River discharge data	Global Runoff Data center (GRDC) (https://www.bafg.de/GRDC/EN/01_GRDC/grdc_node.html).	Gauging stations and time periods: (1) Pandu (1956-1963, 1971-1979); (2) Mathanguri (1955-1964, 1971-1974); (3) Kaunia (1969-1975, 1985-1991); (4) *Bahadurabad (1956-2011)	GRDC, 2021; *Rao et al., 2020
Global polygon for terrain classification	Geospatial Information Authority of Japan (GSI) 2022 (https://gisstar.gsi.go.jp/terrain2021/)	MERIT DEM-90 m (v1.0.3) merging mainly the SRTM3-90 m (v.2.1) and the ALOS (AW3D-30 m) (v.1) and released in June 2022.	Iwahashi and Yamazaki, 2022

3.2 Methodology

The datasets mentioned above have been used to analyze the selected basins' hydro-geomorphic characteristics and sediment connectivity. For this study, each selected basin is divided into three sub-basins (Fig. 1B), upstream (UPS), midstream (MDS), and downstream (DWS), based on the flow length algorithm (Smith, 1997; Cho, 2020)**.** The methodologies of deriving the meteorological factor, morphometric parameters, topographic parameters, and sediment connectivity index are mentioned below with their applicability and limitations. The statistical analyses were mainly performed using software R (version 4.1.0) (R Development Core Team, 2020). Multicollinearity was checked for the morphological and topographic data. Then generalized linear mixed models (GLMMs) were used to analyze the interactive and univariate effects on sediment connectivity, where the "glmmADMB" package was used (Alam et al., 2021).

3.2.1 Meteorological factors

The meteorological studies focus on the TRMM rainfall data analysis because of unevenly distributed and poorly maintained real-time rain gauge data, complicated transboundary issues, and limited accessibility along the Brahmaputra River basin (Shrestha et al., 2008; Bajracharya et al., 2015). Comparative studies of satellite-based and gauge-based rainfall estimation documented that monthly TRMM products are more reliable than other estimations (Huffman et al., 2007; Immerzeel, 2008; Medhioub et al., 2019), where the systematic bias is significantly reduced in the low altitude river basins (Yong et al., 2014). In addition, the gridded rainfall dataset of the India meteorological department (IMD) and gauge rainfall (47 stations) observations of Bangladesh water development board (BWDB) tested the suitability of using the TRMM dataset over the Ganges–Brahmaputra–Meghna river basin (Prasanna et al., 2014). Furthermore, the rain gauge-based validation of the TRMM dataset in the Brahmaputra basin encourages us to use it for meteorological analysis (Shukla et al., 2014; Bajracharya et al., 2015; Tarek et al., 2017). Therefore, TRMM-3B43 version 7 products of 0.25° by 0.25° fine spatial resolution and monthly temporal resolution have been downloaded and processed (Huffman et al., 2007, Huffman et al., 2010; NASA, 2017). These gridded rainfall datasets are available in NetCDF format and converted to raster layer using multidimensional tools of ArcGIS model builder language. TRMM-3B43 products of (mm/h) unit converted to (mm/month) by multiplying the hourly rain rate with the total hours in that particular month and then the annual scale (Shukla et al., 2014). Brahmaputra River discharge datasets accessed in ASCII format at a monthly scale have been converted to annual-scale (m^3/s) for the specific available years.

3.2.2 Geomorphometric factors

The morphometric parameters of linear (stream order, stream length, bifurcation ratio), areal (circularity ratio, stream frequency, drainage density, and compactness coefficient), and relief aspects (basin relief, relief ratio, and ruggedness number) have been computed along with longitudinal profiles. The formula for calculating each morphometric parameter with its respective reference has been provided in Table 3. ArcGIS software analysis has measured the watersheds' areas, perimeter, and length. The channel network was determined by the stream threshold approach with several trials and errors (Jenson and Domingue, 1988; Heine et al., 2004). The reality and consistency of extracted channel network were visualized from Google Earth satellite images and field investigation at Brahmaputra’s tributary (Teesta, Bangladesh). The longitudinal channel profiles were generated to understand the topographic features and channel anomalies (O’Callaghan and Mark, 1984; Ozulu and Gökgöz, 2018).

3.2.3 Topographic factors

Topographic factors such as the topographic wetness index (TWI), the stream power index (SPI), the sediment transport index (STI), the LS (slope-length) factor, and the topographic position index (TPI) have been considered in this study as they provide helpful information about geomorphological characteristics of river basins (Table 3). Furthermore, a range of previous geomorphic studies also applied these factors, notably Pei et al. (2010), De Reu et al. (2013), Papaioannou et al. (2014), Rahmati et al. (2019), and Swarnkar et al. (2020). The topographic indices are often evaluated using geographic information system (GIS) (De Roo, 1998; Chen and Yu, 2011). Our study also uses an ArcGIS model builder language environment to compute rapid topographical analysis of large basins. Different topographic indices for geomorphic characterization largely depend on the quality, availability, and resolution of the DEM (Sørensen and Seibert, 2007; Grabs et al., 2009). Also, it is not certain that increasing DEM resolution will improve topographic indices' performance (Oguchi et al., 2022) as topography has less control over the groundwater flow (Grabs et al., 2009). Here, we used newly released and freely accessible 30-m NASA-DEM as a significant input of topographic factor analysis.

Here, TWI is calculated based on Moore et al. (1993) (Table 3, Eq. (1)), which provides an alternative for understanding the spatial pattern of wetness (Sørensen et al., 2006; Grabs et al., 2009). The SPI reflects the stream power, which is considered here as one of the factors that determine river channel erosion, basin-scale variability in channel processes, morphology, and sediment transport potential (Moore et al., 1991; Pei et al., 2010; Kaushal et al., 2020) (Table 3, Eq. (2)). However, the values of TWI and SPI are influenced by the calculating algorithm of specific catchment area (A_s) and gradient (Tanβ) as the computation of A_s depends on the flow direction algorithm (Chen and Yu, 2011). The STI is calculated by Moore et al. (1991) (Table 3, Eq. (3)) to characterize the erosion and deposition processes (Kalantari et al., 2014; Mojaddadi et al., 2017). Furthermore, the LS factor (dimensionless) reveals the fact that erosion increases with slope angle and slope length (Winchell et al., 2008; García Rodriguez and Giménez Suarez, 2010), and here, it has been calculated by applying a numerical model described by Moore et al. (1991) (Table 3, Eq. (4)). Moreover, TPI measures topographic slope positions and subdivides the landscapes into morphological classes based on topography (De Reu et al., 2013). In the present study, TPI is calculated based on the equation derived by Gallant and Wilson (2000) (Table 3, Eq. (5)) at 2×2 windows as it was successfully applied with field verification at highly sloping hilly terrain in India (Chauniyal and Dutta, 2018). The TPI value ranges from positive to negative values, representing ridges and valleys, respectively, where zero values correspond to flat areas (Gallant and Wilson, 2000; Amatulli et al., 2020).

Here, the functions and computation of morphometric and topographic factors in Table 3 use ArcGIS model builder visual programming language, and are then converted to semi-automated morphometric assessment tools (SMAT) (Supplementary Fig. S2). It has three components (a) a morphometric and topographic assessment tool (MTAT), (b) a longitudinal profile extraction tool (LPET), and (c) a TRMM data extraction tool (TRET). The SMAT tools, developed from the current workflow, shortened the computation time of meteorology (rainfall), morphometric, and topographic parameters and are provided in the supplementary material.

Table 3. Methodology adopted for computing morphologic and topographic parameters

Parameters name	Equation	References
Stream order (u)	Hierarchical rank	Strahler, 1964
Stream number (N_u)	$N_u = N_1 + N_2 + N_3 + ... + N_n$	Horton, 1945
Stream length (L_t) (km)	$L_t = L_1 + L_2 + L_3 + ... + L_n$	Strahler, 1964
Stream frequency (Fs)	$F_s = N_u/A$; Where A is basin area.	Horton, 1932
Bifurcation ratio (R_b)	$R_b = N_u/N_u + 1$; where $N_u + 1$ is number of segments of the next higher order.	Strahler, 1964
Drainage density (D_d) (km/km^2)	$D_d = L_u/A$; where L_u is total stream length of order 'u'.	Horton, 1932
Circularity ratio (R_c)	$R_c = 4\pi \times A/P^2$; Where, A is the area enclosed within the boundary of watershed divide (Basin area)	Strahler, 1964
Compactness coefficient (Cc)	$C_c = 0.2824 \times (P/\sqrt{A})$; where P is the length of the watershed divide which surrounds the basin	Gravelius, 1914
Basin relief (R) (m)	R= Max H – Min H	Strahler, 1952
Relief ratio (R_r)	$R_r = R/L_b$; Where L_b is the distance between the outlet and farthest point on the basin boundary (Basin length).	Schumm, 1956
Ruggedness number (R_n)	$R_n = D_d \times (H/1000)$; Where D_d is drainage density, and H is basin height.	Patton and Baker, 1976
Topographic Wetness Index (TWI)	$TWI = \ln(A_s/\tan\beta)$ … … … … … … … … … … . (1) Where, A_s is the specific catchment area and β is the slope gradient in radians.	Moore et al.,1993
Stream Power Index (SPI)	$SPI = A_s \times \tan\beta$ … … … … … … … … … … … … (2) Where, A_s is the specific catchment area and β is the slope gradient in radians	Moore et al., 1993
Sediment Transport Index (STI)	$STI = (m+1)(A_s/22.13)^m \times (\sin\beta/0.0896)^n$ … … (3) Where, A_s is the specific catchment area ($m^2\ m^{-1}$), β is the slope gradient in degrees, m is 0.4, and n is 1.3.	Moore et al., 1991
LS (slope-length) factor	$LS = (n+1)(A_s/22.13)^n \times (\sin\beta/0.0896)^m$ … … (4) Where, n = 0.4, and m = 1.3	Moore and Burch, 1986
Topographic Position Index (TPI)	$TPI = Z_0 - (1 - nZ_n)/n$ … … … … (5); Where, Z_0 is the elevation of the point under evaluation, Z_n is the elevation of the points within the local window, and n is the total number of surrounding points employed in the evaluation.	Gallant and Wilson, 2000

3.2.4 Index of sediment connectivity

The sediment connectivity index estimates the potential connection or sediment mobilization between the sediments eroded from hillslopes and the stream system, considering the land surface and topographic characteristics (Borselli et al., 2008). The IC was primarily applied in relatively smaller basins covering ~10 to ~150 km^2 with a very high-resolution (~2.5 m) DEM (Cavalli et al., 2013). Mishra et al. (2019) and Swrankar et al. (2020) applied this IC in the larger basin area (~50,000 to 70,000 km^2) of the Ganges with coarser SRTM-DEM (~90 m and ~30 m resolution) to understand the sediment connectivity between hillslopes and channels. Hence, taking encouragement from SedInConnect tool designer Crema and Cavalli (2018) and previous work (Mishra et al., 2019; Zanandrea et al., 2019; Swrankar et al., 2020), this connectivity index is applied to the middle Brahmaputra basin as a novel approach, where sediment dynamics are not fully understood. Here, sediment connectivity analysis is carried out using the stand-alone freely available SedInConnect 2.3 tools (https://github.com/HydrogeomorphologyTools), introduced by Crema and Cavalli (2018). The functionalities and algorithm of the TauDEM 5.3.7 tool (Terrain Analysis Using Digital Elevation Models) (https://hydrology.usu.edu/taudem/taudem5/downloads5.0.html) is used to reflect a more usual pattern of sediment connectivity through the basins (Tarboton, 1997; Cavalli et al., 2013). This connectivity index (IC) is defined as follows:

$$IC_k = log_{10}\left(D_{up}/D_{dn}\right) = log_{10}\left(WS_k\sqrt{A_k}/\sum i = k, n_k\; d_i/W_iS_i\right) \dots\dots (6)$$

where IC_k is the sediment connectivity index (dimensionless) at the particular cell; k is the cell number; D_{up} is the upslope component; D_{dn} is the downslope component; W is an average weight factor (usually considered as C-factor of RUSLE equation, dimensionless) of the upslope contributing area; S_k is the average slope (m/m) of the upslope contributing area at a particular cell (k); A_k is the upslope contributing area (m^2) at cell (k); n_k is the total number of the cell in the basin; d_i is the length of the i^{th} cell along the flow path (m); W_i is the weight (C factor) at the i^{th} cell (dimensionless); S_i is the slope (m/m) at the i^{th} cell. The IC is defined in the range of $[-\infty,+\infty]$, with connectivity increasing for larger IC values.

The calculation of the IC is mainly based on topography. However, land-use cover information can be integrated into the analysis by utilizing weighting factors, e.g., C-factor, as shown by Borselli et al. (2008). We used NASA-DEM (30 m resolution) for topography and channel network as the target. The C-factor is considered as the weight factor generated from the Sentinel-2 derived land-use/land-cover map of 2021, which may provide better insight into the connectivity pattern as heterogeneous landscape favors using the C-factor as weighting factor (Cavalli et al., 2014; Cantreul et al., 2018). The C-factor values of individual cells are acquired from the published literature for a range of land-use/land-cover classes mentioned in Table 1 (FAO, 1978; Wischmeier and Smith, 1978; Morgan, 2009; Ganasri and Ramesh, 2016; Swrankar et al., 2020). Using the C-factor as weight in the IC computation would help us model the impedance to runoff and sediment fluxes from local land use and soil surface (Borselli et al., 2008). Here, both the input layers (i.e., NASA-DEM and C-factor map) are resampled to the same pixel size (30 m) for the calculation of IC (Eq. (6)). According to several researchers (notably Zanandrea et al. (2019); Mishra et al. (2019); Swrankar et al. (2020); Martini et al. (2020); Liu et al. (2021)), this DEM resolution is sufficient to evaluate sediment connectivity. In addition, particle size of sediments is another influential factor for the calculation of sediment connectivity, particularly for a relatively small, steep watersheds with diverse particle size including boulder, gravel, sand, and mud. However, our study focuses on wider areas with less variable sediment particle size (mainly sand and mud), so we assume the effects of differing particle size on the calculated IC in a broader scale is minimal (Garzanti et al., 2004; Fryirs and Brierley, 2013). Therefore, the IC values derived from topography and land-use/land-cover characteristics would help us to better understand the sediment connectivity pattern in these large basins.

4. Results

4.1 Geomorphometric analysis

The result of geo-morphometric parameters are presented in Table 4. The Strahler's stream order suggests that 7^{th} (Teesta), and 8^{th} (Torsa and Manas) order stream networks are present along these basins (Fig. 3A). Compared to the midstream and upstream sub-basins, higher stream frequencies have been observed downstream (Fig. 3B). Considering the whole basin (WB), the stream frequency ranges from (1.12 to 1.14 km^{-2}) where the highest stream frequency is found at Teesta (1.14 km^{-2}) compared to others. High stream frequency, larger catchment area, and high discharge in downstream areas may suggest the dominancy of channel processes and, therefore, more erosion (Fryirs and Brierley, 2013; Oyedotun, 2020). Drainage density is related to climate, the type of rocks, relief, vegetation cover, surface roughness, and several hydrological processes such as infiltration capacity, soil saturation, and overland flow, which impact the production of runoff and sediment load in the basin (Rudraiah et al., 2008; Swarnkar et al., 2020). For the whole basin, the drainage density (D_d) results suggest comparatively higher values in the Teesta basin (1.07 km/km^2) compared to the Torsa basin(0.98 km/km^2), and the Manas basin (0.96 km/km^2) (Fig. 3C). The variability of infiltration numbers shows the dominancy of MDS and DWS over the UPS except for the Manas basin. The infiltration number is relatively higher in the whole basin of Teesta (1.21) compared to Torsa (1.10), and Manas (1.08). This result infers that the Teesta basin has a lower infiltration capacity with high runoff, followed by the Torsa and Manas basin because the infiltration number implies that the higher the value of the infiltration number, the lower will be the infiltration with higher runoff (Bhatt and Ahmed 2014). The result of the compactness coefficient (C_c) for the whole basin shows the highest values in Manas (3.43), whereas the lowest is found for Torsa (2.95). In the whole basin, the circulator ratio (R_c) ranges from 0.16 to 0.24, where higher values are found for Manas (0.24), followed by Torsa (0.23), and Teesta (0.16). The circulatory ratio varies from 0 to 1 (where a higher value shows a more circular basin shape) (Miller, 1953). The low values for the circulatory ratio in these basins indicates that basin shapes are not circular and suggests that they reflect an early stage of topographical maturity, which may significantly affect their hydrological response (Rai et al., 2017). High variations of bifurcation ratio have been observed from upstream to downstream sub-basins, where the highest bifurcation ratio has been observed in the MDS of Teesta (2.27) (Fig. 3D). As a whole basin, Teesta shows a relatively higher bifurcation ratio (R_b) (1.87) compared to the Manas (1.75) and Torsa (1.77) basins. Bifurcation ratios between 3 and 5 means the drainage system is less influenced by tectonics (Strahler, 1964), therefore, values in this study (<3-5) infers the dominance of modern geomorphic processes rather than tectonics.

The basins in this study are characterized by a large basin relief, which is highest in Teesta (7901 m) followed by Manas (7490 m) and Torsa (7208 m), and indicates the steepness of these basins (Parveen et al., 2012; Rai et al., 2017). The relief ratio (R_r) of the Teesta, Torsa, and Manas basins is 6.61, 6.36, and 5.69, respectively (Fig. 3E). The relief ratio has a direct relationship with slope gradient, so the relief ratio of the Torsa and Teesta basins is also high (Rudraiah et al., 2008). For the whole basin, the ruggedness number (R_n) varies from 7.07 to 8.42. Teesta shows higher values (8.42), which implies more rugged terrain compared to other basins (Patton and Baker, 1976; Debelo et al., 2017). The variation in R_n values reflects slope and relief differences among these sub-basins and basins.

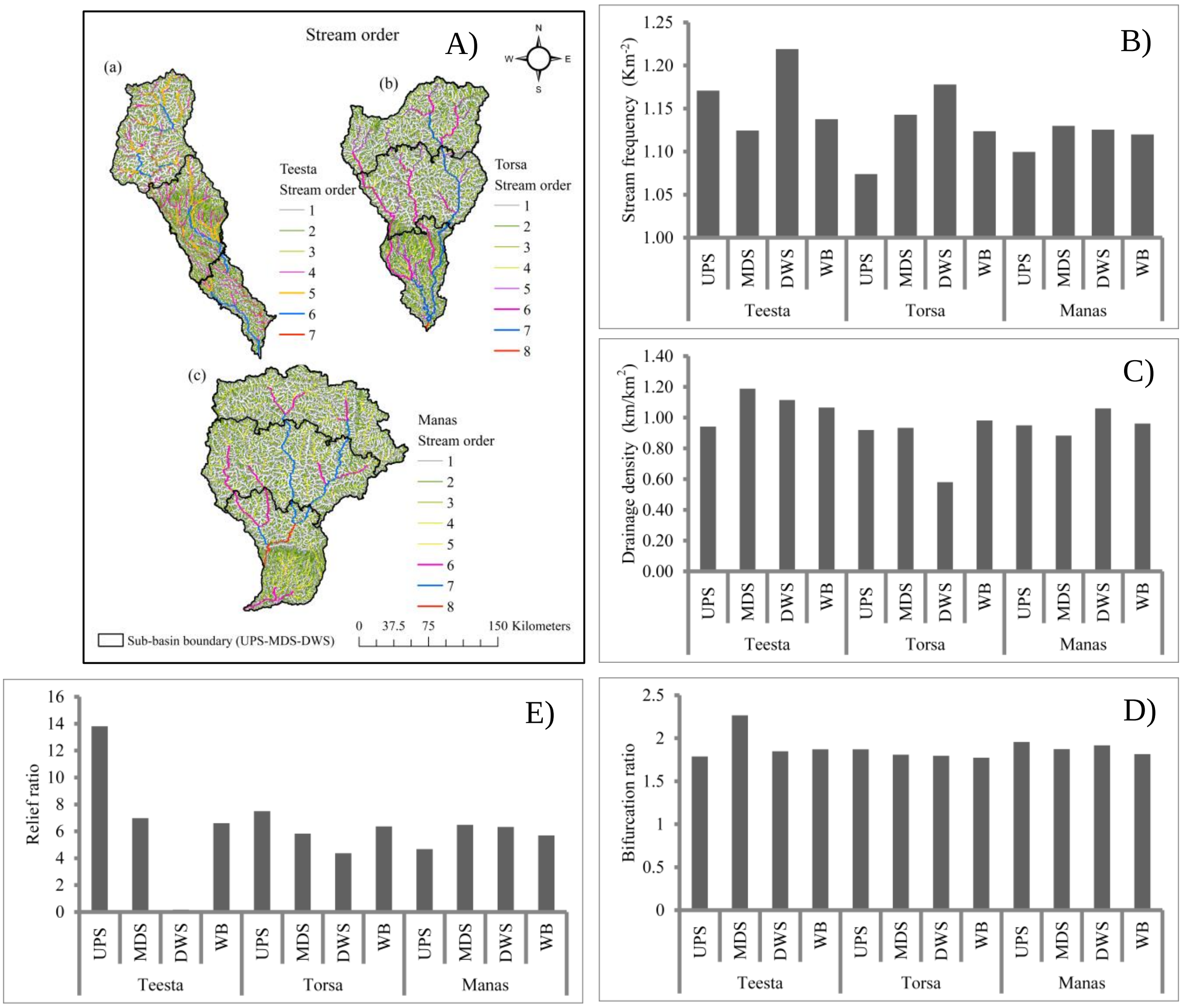

Fig. 3. A) Stream order (Strahler, 1964) maps for (a) Teesta, (b) Torsa, and (c) Manas basin. Bar plots of B) stream frequency, C) drainage density, D) bifurcation ratio, and E) relief ratio are shown for all the basins and sub-basins.

Table 4. Comparison of morphometric parameters at selected basins and sub-basins

Basin	Sub-basin	F_s	R_b	R_c	D_d	D_t	C_c	If	R	R_r	R_n
Teesta	UPS	1.17	1.79	0.20	0.94	1.10	1.49	1.10	7901	13.80	7.44
	MDS	1.12	2.27	0.20	1.19	1.34	1.62	1.34	4336	6.98	5.15
	DWS	1.22	1.85	0.13	1.11	1.36	1.44	1.36	99	0.18	0.11
	WB	1.14	1.87	0.16	1.07	1.21	3.12	1.21	7901	6.61	8.42
Torsa	UPS	1.07	1.87	0.18	0.92	0.99	2.08	0.99	5981	7.49	5.50
	MDS	1.14	1.81	0.18	0.93	1.07	2.11	1.07	4726	5.83	4.41
	DWS	1.18	1.80	0.18	0.58	1.35	1.58	1.35	2656	4.37	3.05
	WB	1.12	1.77	0.23	0.98	1.10	2.95	1.10	7208	6.36	7.07
Manas	UPS	1.10	1.96	0.13	0.95	1.04	2.64	1.04	4736	4.67	4.50
	MDS	1.13	1.87	0.22	0.88	1.00	2.79	1.00	6944	6.49	6.13
	DWS	1.13	1.92	0.22	1.06	1.19	1.83	1.19	4444	6.32	4.71
	WB	1.12	1.82	0.24	0.96	1.08	3.43	1.08	7490	5.69	7.20

Note: abbreviations of parameters are according to Table 3.

4.1.1 Longitudinal profiles analysis

The longitudinal profile depicts the change in the channel bed elevation over the river's entire length from its origin to its mouth (Rhoads, 2020). Fig. 4 shows that longitudinal profiles are concave-upward to relatively flat. The upstream region in these basins mostly shows a steep profile with sharp transitions. The Teesta, Torsa, and Manas's midstream region mainly shows gradually decreasing profiles. In contrast, almost flat segments with irregularities are observed in downstream areas, where the elevation change is limited but might be very sensitive to depositional characteristics. The deviations of the most observed concave nature of long profiles with irregularities in these basins may depict the response of long profiles to tectonics, change in base level, water discharges, and sediment load characteristics of these basins (Goswami, 1985; Whipple and Tucker, 1999; Jiang et al., 2016). The errors or irregularities along the valley bottom profiles may arise from converting discrete altitude measurements into gridded elevation information of coarse-grained (10 to 30 m resolution) DEM data (Hayakawa and Oguchi, 2006; Schwanghart and Scherler, 2017; Rhoads, 2020).

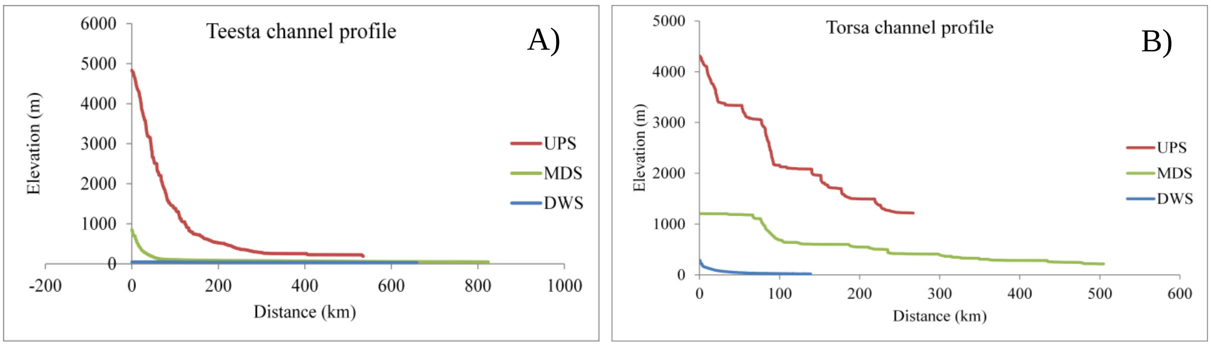

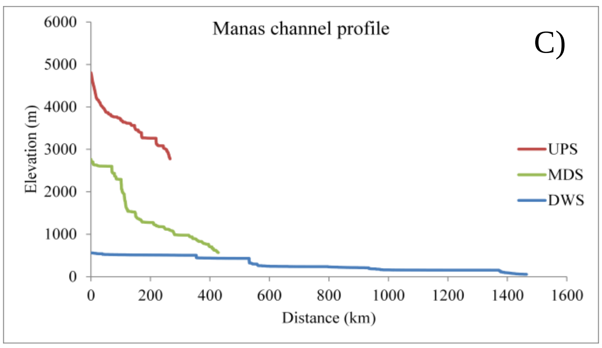

Fig. 4. Longitudinal channel profiles of A) Teesta, B) Torsa, and C) Manas. UPS, MDS, and DWS reaches have been considered to show the variations in channel profiles. The distance is from the upstream end of each section.

4. 2 Topographic analysis

The topographic factors are described from upland to downslope areas in Table 5. Generally, a channel slope greater than 25° is preferred for debris or sediment flow initiation, which decreases with increasing catchment area (Takahashi, 1981; Hungr et al., 1984; Rickenmann and Zimmermann, 1993; Van Dine, 1996). Here, in the upstream region, the average slope is greater than 25° except at Manas (23.41°) basin. The slope in the midstream region drops drastically at Teesta (7.97°). Downstream, the lowest slope is found for Teesta (1.72°), followed by Torsa (4.31°) and Manas (17.24°). The average slope varies significantly across the whole basin, where a higher gradient is found for Manas (23.76°), followed by Torsa (21.78°) and Teesta (16.13°). The slope difference at the whole basin scale shows that with a steeper slope, Manas has a relatively higher potential for flow or sediment initiation than the Torsa and Teesta basins. Overall, the gradient varies highly, reflecting the heterogeneous terrains' behavior. Slope significantly controls complex terrain's erosion and deposition potential (Rafaelli et al., 2001), and the head area slope generally determines the sediment delivery (Fontana and Marchi, 1998). The runoff, sediment yield, or sediment transport capacity increased as the slope gradient increased (Xiao et al., 2017; Jourgholami et al., 2021). Here, the steeper slope has been observed in the upstream areas, showing the potentiality for flow or sediment initiation. In contrast, the slope decreased dramatically along the midstream and downstream reaches, reducing the sediment connectivity or transport potential and favors deposition.

Further, the TWI has been used to assess the presence of saturation, which is essential for ephemeral gully formation (Foster, 1990) and influences the runoff processes and suspended sediment flows (Sharma, 2010). Generally, large TWI values are seen at the lower slope or on the valley floor of large catchment areas. Here, TWI at UPS varies from 5.80 to 6.10, with the highest values in Manas (6.10). In the midstream and downstream reaches, the

TWI ranges from 5.79 to 7.63 and 6.93 to 8.55, respectively, where comparatively higher values are found in downstream reaches. As for the whole basin, the highest TWI has been found for Teesta (7.00), followed by Torsa (6.37) and Manas (2.15). The steeper slope upstream and high TWI at the downstream zone of the Manas basin can initiate high flows compared to Torsa and Teesta basins. Moreover, a significant positive relationship between TWI and slope suggests high sediment flow potential at UPS because of a higher gradient and lower TWI. In contrast, DWS suggests lower sediment flow caused by a steeper slope and higher TWI (Fig. 5A). The analysis of TWI illustrates that high values are mostly found along the downstream region (mostly flat terrain) while low values are typical in the upstream region (mostly steeper terrain). Therefore, the areas with high TWI (i.e., downstream) will have a greater risk of gully erosion than areas with low TWI value (i.e., upstream) (Sharma, 2010).

Furthermore, the SPI has been used to evaluate the erosion and potential energy of overland flow that is available to cause sediment transport where a high SPI indicates a more significant potential for soil erosion (Moore et al., 1993). Upstream, the SPI ranges from -1.19 to -1.02, where the highest values are found for Teesta (-1.02), followed by Torsa (-1.13), and Manas (-1.19). At midstream and downstream areas, the SPI ranges (-4.09 to -0.91) and (-4.98 to -2.63), respectively, where higher values are found in Manas, followed by Torsa and Teesta. Similarly, in the whole basin, the highest SPI values are found in Manas (-1.43), followed by Torsa (-1.87) and Teesta (-1.87). Intra-basin comparison shows that upstream sub-basins show comparatively higher SPI values, possibly caused by higher elevation. The significant positive relationship between slope and SPI depicts its high potential at UPS (high slope, high SPI) and lower potential at DWS (low slope, low SPI) for sediment transport (Fig. 5B). Furthermore, the steeper slopes with high SPI and low TWI are expected to have high flow and sediment potential. High SPI with steeper slopes at upstream reaches of the Teesta, Torsa, and Manas basins can initiate high flows, but low SPI and high TWI with flatter slope downstream may imply the sediment deposition within the channel.

The STI of upstream areas varies from 0.65 to 0.39, and higher values have been observed in the Manas basin. In midstream and downstream regions, the STI ranges from 0.42 to 0.65 and 0.39 to 0.63, respectively. For the whole basin, Teesta, Torsa, and Manas show similar values (0.68). The low STI value at downstream reflects the slow mobility and, consequently, the accumulation of sediments. Furthermore, a high LS factor value suggests a higher rate of soil loss (Vijith and Dodge-Wan, 2019). The LS factor values at UPS range from 0.16 to 0.26, where higher values are found in Manas, followed by Torsa (0.16) and Teesta (0.16). At MDS and DWS, the LS values range from 0.17 to 0.25 and 0.20 to 0.29, respectively. Inter-basin comparison of LS values shows that Teesta has a higher LS value (0.31) compared to Torsa (0.29) and Manas (0.28). High LS and STI values are expected to initiate the high erosion and flows at the UPS zone, whereas the MDS and DWS may experience deposition scenarios. The LS factor directly impacts erosion and transport potential from the source region to downstream, where a high LS factor value shows greater potential (i.e., UPS of Teesta) (Arabameri et al., 2018; Vijith and Dodge-Wan, 2019). Previous studies by Das et al. (2022) found a similar trend of LS values in the Indian Himalayan region.

The application of TPI is limited in the Himalayan region (Chauniyal and Dutta, 2018). Here, TPI is estimated to infer the slope pattern and landforms of the study area. According to Weiss (2001), the landform can be classified as ridges: TPI > 1.0, upper slope: 1.0 > TPI > 0.5, middle slope: 0.5 > TPI > -0.5 (angles greater than 15°), flat: 0.5 > TPI > -0.5 (angles less than 15 °), lower slope: -0.5 > TPI > -1.0, and valley: TPI < -1.0. In our study, the TPI varies from -1.67 to 0.33, -0.77 to 0.37, and -0.92 to 0.30 in upstream, midstream, and downstream, respectively. Here, the negative TPI values are found in Teesta and Torsa from upstream to downstream. The positive values of TPI from upstream to downstream in Manas depict its ridge formation, while the negative values in Torsa and Teesta reveal its valley formation. However, as a whole basin, none of the basins has negative values of TPI, where the highest values are found for Teesta (0.22) followed by Torsa (0.12) and Manas (0.10). The TPI values of the whole basin fall within the range 0.5>TPI<-0.5, which identified these basins as middle slope regions, where UPS and DWS are dominated by a steeper slope and a lower slope, respectively. Roy and Das (2021) classified a similar pattern of landforms conducted in the eastern Himalayan catchment near the Brahmaputra's northernmost tributary (Teesta). The TPI result shows large variations in topography though the results may vary because of the basin's radius, scale, or surface roughness (Grohmann and Riccomini, 2009). Here, the spatial distribution of TPI illustrates the formation of upper slope to valley-type landforms where the sediment may accumulate at DWS because of the flat landscape (Gallant and Dowling, 2003).

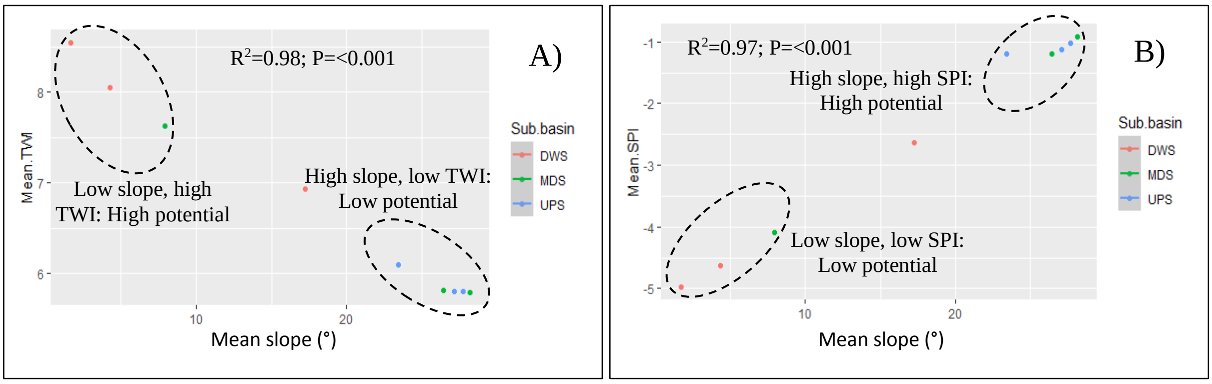

Fig. 5. Relationship of topographic features A) mean slope and mean TWI; B) mean slope and mean SPI in each UPS, MDS, and DWS sub-basins. The slope is in degrees.

Furthermore, this study's topographic features (i.e., TWI and SPI) show significant correlations with the standardized terrain geometric signatures (ZLnslope, ZLnHAND, and ZTexture) that represent the ground feature efficiently (Iwahashi et al., 2021; Iwahashi and Yamazaki, 2022). This correlation represents the validity of topographic patterns obtained from the present study (Fig. 6). Moreover, he terrain classification map in Fig. 7 represents the hilly mountainous to the lowland features, resembling the spatial distribution of topographic features derived from this study.

Table 5. Basin topographic features analyzed (abbreviations are according to Table 3)

Basin	Sub-basin	Slope (degree)	TWI	SPI	STI	LS	TPI
Teesta	UPS	27.70	5.80	-1.02	0.39	0.16	-1.67
	MDS	7.97	7.63	-4.09	0.46	0.23	-0.67
	DWS	1.72	8.55	-4.98	0.42	0.21	-0.19
	WB	16.13	7.00	-2.75	0.68	0.31	0.22
Torsa	UPS	27.12	5.80	-1.13	0.39	0.16	-1.34
	MDS	26.43	5.81	-1.19	0.42	0.17	-0.77
	DWS	4.31	8.05	-4.63	0.39	0.20	-0.92
	WB	21.78	6.37	-1.87	0.68	0.29	0.12
Manas	UPS	23.41	6.10	-1.19	0.65	0.26	0.33
	MDS	28.14	5.79	-0.91	0.65	0.25	0.37
	DWS	17.24	6.93	-2.63	0.63	0.29	0.30
	WB	23.76	2.15	-1.43	0.68	0.28	0.10

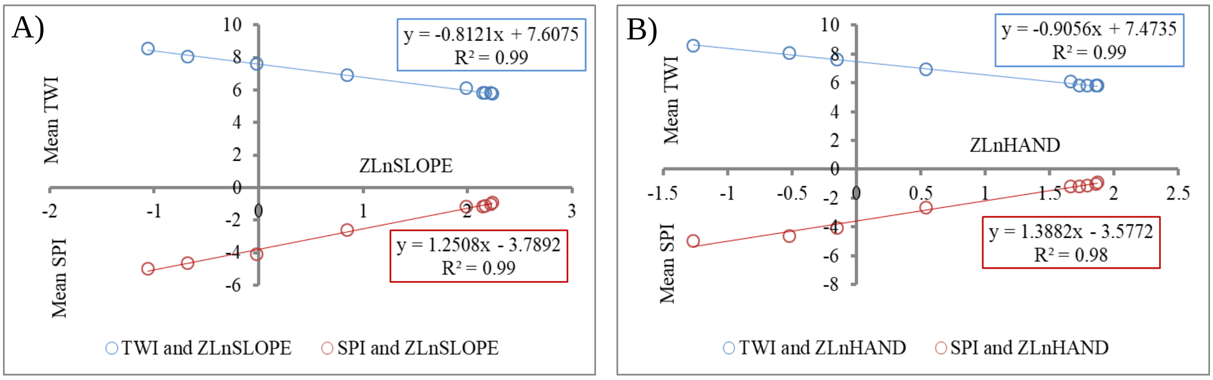

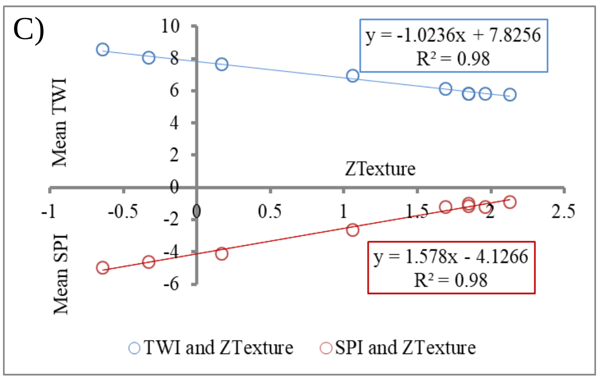

Fig. 6. Correlation of terrain geometric signatures and topographic features A) ZLnslope with TWI and SPI, B) ZLnHAND with TWI and SPI, and C) ZTexture with TWI and SPI. P<0.001 shows a significant level.

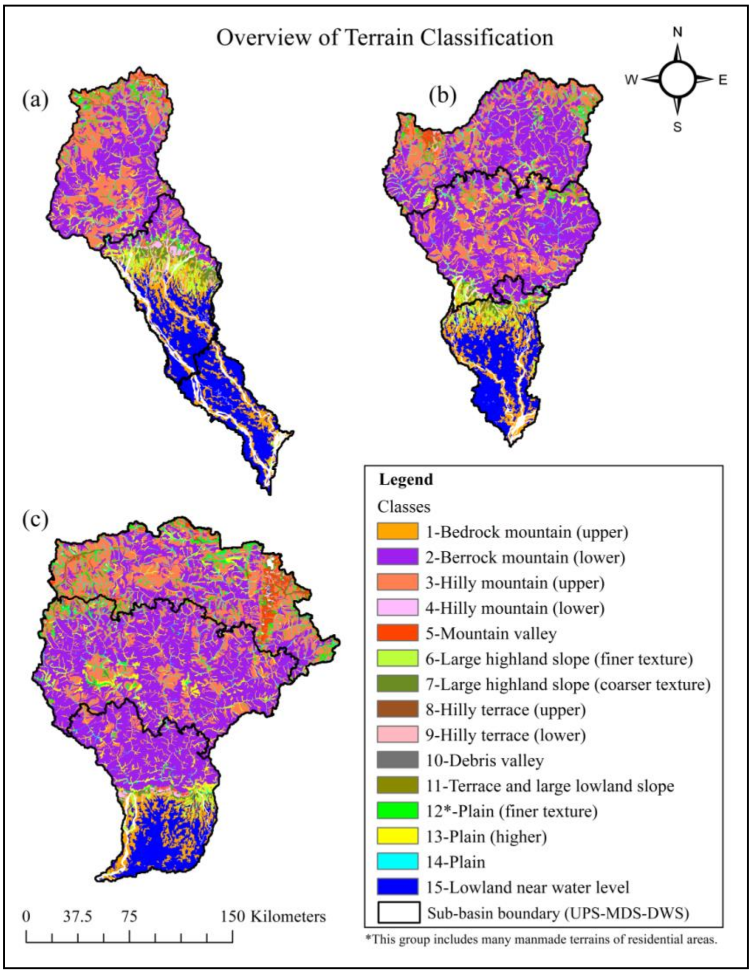

Fig. 7. Terrain classification with geomorphological features of a) Teesta, b) Torsa, and c) Manas basin based on the data of Iwahashi and Yamazaki (2022).

4.3 Index of connectivity (IC) analysis

4.3.1 Spatial analysis of IC

The spatial IC patterns of studied basins show non-homogenous connectivity potentials (Fig. 8). The region close to the channel network represents the higher potential connectivity and the area far from the channel network generally shows lower connectivity potential. The pattern of sediment connectivity is essential in large-scale river basins because the degree of connectivity is fundamental to understanding the response to natural and anthropogenic disturbances (Wohl et al., 2019). The distribution and descriptive statistics of IC values for different basins are presented in Fig. 9 and Table 6, respectively**.**

The inter-sub-basin comparison of IC values shows that higher IC values have been observed mainly along the UPS zone rather than along the MDS and DWS zones. The higher mean IC values (>-6.55) along the UPS zone represent higher potential connectivity within the channel because of high hillslope slopes from upstream areas. In the MDS and UPS reaches, higher values are observed compared to the DWS, which shows moderate to low (<-6.92) IC values. Compared with UPS, the mean IC values at MDS are decreased by 0.53, 0.67, and 1.36 in Teesta, Torsa, and Manas, respectively. Also, at DWS, the mean IC value is reduced by 0.45, 1.90, and 1.94 in Teesta, Torsa, and Manas, respectively, compared to UPS. The decreased mean IC values from UPS to MDS and DWS reflect the decrease in sediment connectivity in these basins. The IC variations from upstream to downstream are distinct, with high and slightly connected areas visible to higher and lower slope areas. Higher slopes in the UPS zone and agriculture patches or built-up areas along the DWS zone may contribute to high IC variations from its upstream to downstream (Mishra et al., 2019; Swarnkar et al., 2020).

Furthermore, the inter-basin comparison shows higher IC values for Manas (-6.52), followed by Torsa (-7.09) and Teesta (-7.30). The difference in mean IC values among these basins is not so high but still distinctive. The connectivity pattern may be attributed to the upstream-downstream linkage of the basin, where topography and land use play a dominant role. However, lower IC values along the DWS of Torsa (-7.50) and Teesta (-7.02) show disconnected terrain, affecting the overall sediment connectivity or routing in these basins. The lower average annual discharge (1001 m^3/s) at Kaunia (Bangladesh) station from (1985 to 1991) and the decrease of water flow at Dalia point from (1985 to 2006) (Mondal and Islam, 2017) of Teesta can confirm the lower IC values and lower connectivity potential at the DWS of Teesta (Supplementary Fig. S1E). In addition, the anthropogenic disturbances along the Teesta basin were reported in several cases (Khan and Islam, 2015; Goyal and Goswami, 2018), which may significantly affect these basins' sediment connectivity and transport.

The differential IC values suggest varied connectivity where the UPS are slightly better connected and, hence better or more efficient sediment transport than MDS and DWS. The lower IC values along the DWS suggest a poorly developed channel and lower sediment transport efficiency because of valley-shaped landforms and a more downward slope favoring deposition. The significant standard deviation of IC values also illustrates the variability of connectivity patterns among these basins (Table 6).

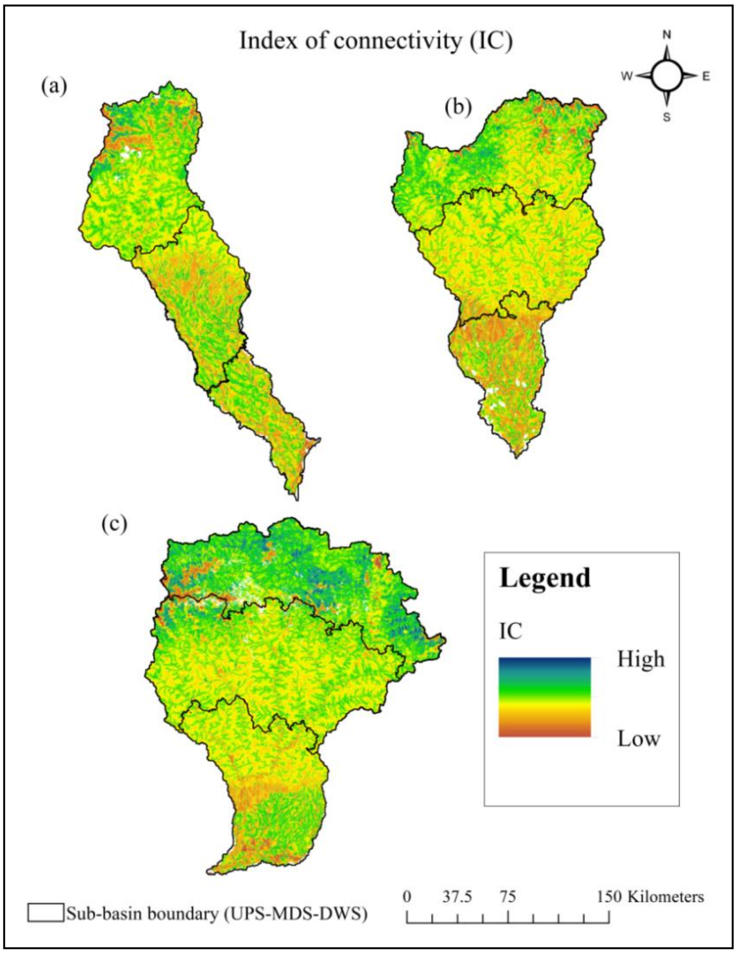

Fig. 8. Spatial distribution of index of connectivity for (a) Teesta, (b) Torsa, and (c) Manas basin.

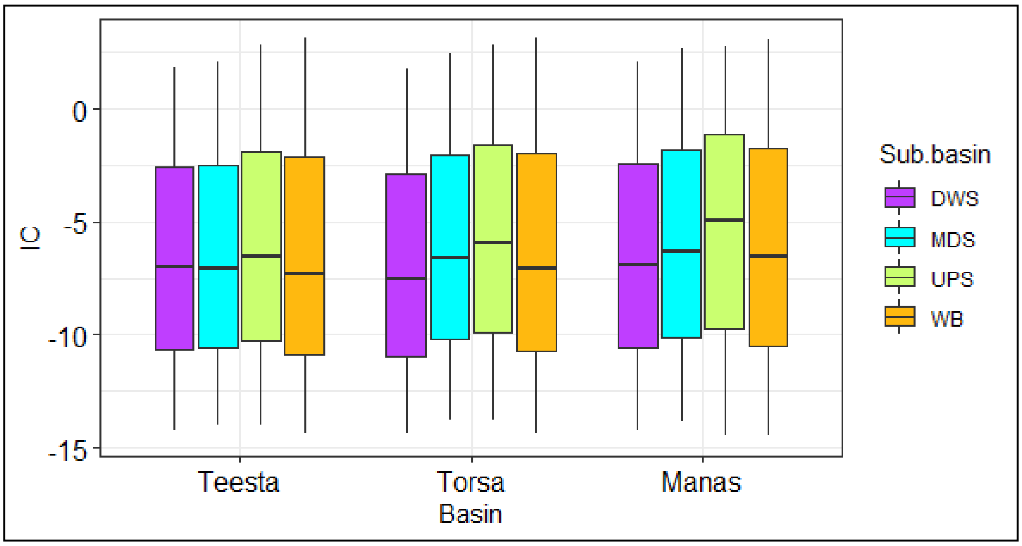

Fig. 9. Distribution of IC for each basin and sub-basins are shown in Box plots.

Table 6. Descriptive IC statistics of studied basins

Basin	Sub-basin	Min	Max	Mean	Std.
Teesta	UPS	-14.02	2.80	-6.55	1.89
	MDS	-14.01	2.08	-7.08	2.02
	DWS	-14.21	1.81	-7.02	2.22
	WB	-14.42	3.10	-7.30	1.94
Torsa	UPS	-13.77	2.79	-5.96	1.91
	MDS	-13.78	2.47	-6.63	1.27
	DWS	-14.39	1.75	-7.50	2.15
	WB	-14.39	3.09	-7.09	1.73
Manas	UPS	-14.48	2.76	-4.98	2.27
	MDS	-13.83	2.70	-6.34	1.54
	DWS	-14.21	2.08	-6.92	1.88
	WB	-14.49	3.06	-6.52	1.96

4.3.2 Connectivity index and ground-based evidence

Positive correlations between the magnitude of the hydrological process and the sediment connectivity or transport were reported in several earlier studies (Hu et al., 2019; Arabkhedri et al., 2021; Zanandrea et al., 2021). Correlations between mean IC values and the ground-based average annual yield of respective basins, collected from the IUCN physical assessment report on the Brahmaputra River basin prepared from the India-Bangladesh joint field investigation (Mahanta et al., 2014; Pangare et al., 2021), however, shows a slightly negative correlation (Fig.10A). On the other hand, the mean IC values plotted against the geometric signatures (ZlnSLOPE, ZlnHAND, and ZTexture) of terrain classes, which is a proxy for the topographic application and the sediment supply potential (Iwahashi et al., 2021), show positive correlations (Fig. 10B). Although the sample size of this study is too small to statistically validate the results, these may suggest that the relationships between sediment connectivity and yield may not follow the general trend in large-scale basins. For this, more data collection of IC and site-specific ground-based sediment yield observation would be required.

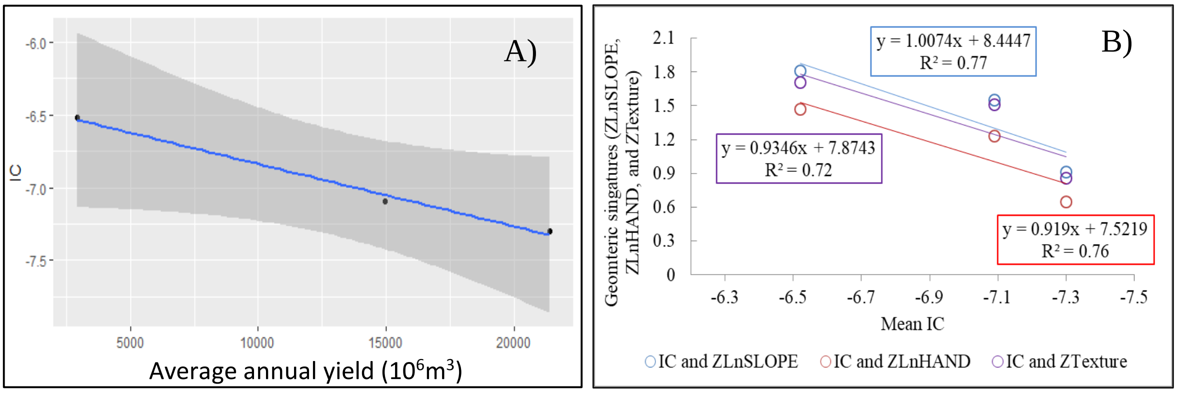

Fig. 10. Correlations between A) mean IC and ground-based average annual yield (blue line and gray shading denote the regression line and 95% confidence interval, respectively), and B) Mean IC and geometric signatures of terrain classes (P value<0.05).

4.4 Inter-relationship among morphometric and topographic variables

Like the morphometric studies of Faghih et al. (2015), Pant et al. (2020), and Różycka and Migoń (2021), correlation analysis has been performed here to examine interrelationships among fifteen (15) different morphometric and topographic variables. Pearson's correlation is frequently used for this purpose and the results of the correlation matrix are given in Supplementary Fig. S3. The correlation matrix of morphometric and topographic variables depicts a significant positive correlation between D_t-F_s, F_s-If, If-D_t, Cc-R_n, slope-SPI, and STI-TPI. Also, significant negative correlations between slope-D_t, slope-TWI, If-SPI, and TWI-SPI have been observed. Various positive and negative correlations depict the interrelationship and importance of these parameters for characterizing the basin.

In addition, the GLMMs test signifies the effect of morphometric and topographic factors (independent variable) on sediment connectivity (IC) (response variable), where SPI shows the best fit model (lower AIC) compared to other factors (Supplementary Table S1). The Akaike information criterion (AIC) is considered an estimator of a model's relative goodness fit for a given dataset, where the lower AIC value represents the best model (Akaike, 1974).

5. Discussion

5.1 Morphometric characteristics of the basin

Noticeable differences in the morphometry of stream network, drainage density, stream frequency, bifurcation ratio, relief ratio, and longitudinal profiles determine the hydro-geomorphic response of individual basins. These basins generally show a higher stream order of 7^{th} to 8^{th} with the dominance of first order streams indicating the existence of a highly permeable lithology leading to a lower infiltration rate, suggesting greater discharge potential (Bindu et al., 2012; Oyedotun, 2020). The average annual discharge of 21,434 m^3/s at Bahadurabad (Bangladesh) station from 1956 to 2011 can validate the discharge potentialities of these basins. The lower mean bifurcation ratio of <3 shows that these basins that are not much influenced by tectonics and geological structure (Sreedevi et al., 2009; Arulbalaji and Gurugnanam, 2017). The drainage density values from our study (range: 1.19 to 0.96) may result from the weak or impermeable subsurface material, sparse vegetation, and mountainous relief (Ozdemir and Bird, 2009; Kanhaiya et al., 2018). The low or moderate slope in downstream areas leads to a higher drainage density, whereas the lower drainage density characterizes a steeper slope at upstream reaches in these basins. As a result, lower surface runoff may be experienced downstream, but an opposite hydrological situation may occur in upstream regions. The drainage density is positively correlated with the relief and erosion process (Sangireddy et al., 2016; Oyedotun, 2020), rapid storm event runoff (Montgomery and Dietrich, 1989; Tucker and Bras, 1998), and hence the sediment supply to the fluvial network (Clubb et al., 2016). However, higher drainage density in these basins may result in potential hydrological responses such as high catchment runoff and potential sediment supply to the downstream fluvial system. The high basin relief of Teesta (7901 m), Manas (7490 m), and Torsa (7208 m) that suggest steepness, accompanied by higher rainfall patterns (Table 1), may determine the hydro-geomorphic characteristics, including flood pattern, erosional processes, and sediment transport in these basins (Hadley and Schumm, 1961; Burrough et al., 2015). Thus, the high relief ratio of these basins may intensify the erosion processes and increase the sediment transport capacities that are produced by upstream portions. Various morphometric features discussed here may significantly control geomorphological processes and the hydrological behavior of downstream areas.

The upstream region shows a mostly steepened longitudinal channel, indicating the potential erosion and sediment transport from the upstream headwater region. Our sediment connectivity analysis also suggests higher IC and connectivity potential at most upstream reaches than midstream and downstream. The channel steepness patterns and irregularities show that the studied basins are erosional landscapes controlled by regional tectonic uplift, water, and sediment discharge (Goswami, 1985; Shi et al., 2020). Downstream, mostly dissecting profiles with errors or irregularities have been observed where the elevation change is limited but may be sensitive to the deposition of sediment. It can also be assumed that, after traveling a long distance, the sediments may be deposited in downstream areas, which are the characteristics of riffle-pool sequences at lowland rivers (Wohl and Merritt, 2008; Rhoads, 2020). The typical concave profiles associated with downstream decreases of elevation characterize the wider valleys, which may impede sediment connectivity and transport potentials of these basins. With the decline of gradient in the downstream direction, the main channel of the Brahmaputra basin receives sediment inflow from many tributaries, creating a possible clogging of the sediment, giving it an intensely braided character (Rajbanshi et al., 2022). The excessive channel deposits, locally called chars (river islands) visualized from the field investigation, are typical characteristics of a braided river that may significantly alter the geomorphology of Brahmaputra's channel planform (Takagi et al., 2007; Rajbanshi et al., 2022).

It is known that the topographic factors affect the sediment discharge and connectivity in a river basin (Cheng et al., 2017). The responses of different topographic factors suggests that steep slopes with high SPI, STI, and lower TWI are expected to have high sediment connectivity and transport potential in the UPS region. On the other hand, a more gently sloping basin with lower SPI, STI, and higher TWI shows lower sediment connectivity and transport potentials at midstream and downstream favoring deposition. The recent field investigation at Teesta downstream in Bangladesh also reveals the presence of depositional features, where bankline erosion is widespread and sediments accumulated (Fig.1C-D). Furthermore, the terrain classification data of Iwahashi and Yamazaki (2022), proxy to the topographic applications, correlates significantly with our study's topographic pattern and effectively reflects our observations. However, topographic factors derived from a 30–m

DEM resolution may affect the values of the indices, which can be investigated in future research (Chen and Yu, 2011; Panagos et al., 2015).

5.2 Sediment connectivity of the basins

In geomorphology, sediment connectivity studies are valuable to understand the sediment dynamics (Heckmann et al., 2018; Wohl et al., 2019), characterizing the geomorphic system (Buter et al., 2022), and addressing geomorphic vulnerabilities (Alca´ntara-Ayala, 2002), which is considered here for understudied Brahmaputra River. The meteorology, drainage basin and topographic characteristics, and connectivity index affect the sediment dynamics of these basins (Table 7). The spatial mapping of hillslope to channel connectivity shows considerable variations and inhomogeneity in these basins (Fig. 8). The slopes, debris fans, and alluvial plains are considered key drivers influencing the sediment conveyance from hillslope to channel within the sediment cascade (Fryirs et al., 2007; Messenzehl et al., 2014). Here, the presence of bedrock mountains, mountainous valleys with large highland slopes, and lowlands near the water table from upstream to downstream might be one reason for such an inhomogeneous connectivity pattern in these basins (Sharma et al., 2012). However, limited ground-based average annual yield data, field investigations, and quantitative geometric signatures based terrain classification greatly support our sediment connectivity analysis.

High IC values with higher slope, SPI, and STI depict a highly connected zone (coupled with stream network) along the UPS, resulting in increased sediment transport efficiency as mentioned by previous studies (López-Vicente et al., 2013; Jing et al., 2022). The high IC pattern in the upstream region corresponds with the presence of highland slopes, hilly mountains, and steep valleys (Sarma, 2004; Singh, 2007; Iwahashi et al., 2021). On the other hand, low IC values with lower slope, SPI, and STI along the MDS and DWS depict a minimally connected zone where the transported sediments maybe deposited. These lower IC values indicate the propensity of these areas to be decoupled from the stream network because of gentler slopes and longer flow paths (Fryirs et al., 2007). The considerable number of large and mid-channel bar developed along with bank migration within the studied basin (Singh, 2007; Sharma et al., 2012; Ashworth and Lewin, 2012), especially in middle and downstream areas, may configure lower connectivity aspects, which may alter the Brahmaputra's planform characteristics (Rajbanshi et al., 2022). In turn, the frequent changes of channel planform may influence the basin-scale geomorphology (Rajbanshi et al., 2022) and increase flood risks (Rao et al., 2020), which is predicted based on Brahmaputra's basin hydrology (Alam et al., 2016) and sediment flux (Rahman et al., 2018).

The upstream-downstream linkages of geomorphological processes in Himalayan River basins were severely impacted by anthropogenic structures, i.e., channel diversions, hydroelectric projects, dams, embankments, etc. (Nepal et al., 2014). The dams in Ganga–Brahmaputra control the discharge, which caused a 31% reduction in its downstream sediment contribution compared to the past and is expected to be aggravated in the future (Gupta et al., 2012; Higgins et al., 2018; Bandyopadhyay et al., 2023). The anthropogenic disturbances on the large river systems may result in the reduction or loss of connectivity and the nature of sediment supply (Jain and Tandon, 2010; Fryirs and Brierley, 2013; Sinha and Ravindra, 2013; Oyedotun, 2016). Hence, the anthropogenic modifications (hydroelectric projects, dams, barrages, channel diversions, hydro-engineering structures) noticed along the studied basins (Supplementary Fig. S4) may decrease sediment connectivity or (dis)connectivity in the mid-to-downstream region and potentially reduce the flow-sediment flux to the main channel. For instance, the diversion of upstream water of the Teesta basin by Gozoldoba (India) and Teesta barrage (Bangladesh) led to a severe water shortage and the channel drying up in downstream Bangladesh (Mondal and Islam, 2017; Goyal and

Goswami, 2018; Singh et al., 2021; Pangare et al., 2021) (Supplementary Fig. S5). Hence it might be one of the reasons for the substantial decrease of sediment connectivity of Teesta at MDS and DWS compared to the upstream areas. Also, the alternation of the natural flow of the Torsa and Manas rivers caused by hydro-engineering structures was reported earlier, which might influence the decreased sediment connectivity along the midstream and downstream regions of these basins (Sharma et al., 2012; Yasuda et al., 2017; Higgins et al., 2018; Saha and Bhattacharya, 2019). The study of Poeppl et al. (2017) underlines the impacts of human-induced alternation of fluvial processes, connectivity, and geomorphic changes in the catchment systems, but are beyond the scope of this article.

Furthermore, land cover directly affects sediment connectivity (López-Vicente et al., 2013; Llena et al., 2019), and here the decreased connectivity from the up-to-downstream region may be attributed to the presence of high vegetation coverage and lower agricultural patches or barren land (Table 1), which may potentially impede the sediment transfer. The heterogeneities of the spatial pattern of sediment connectivity presented in this study can have drastic impacts on the overall behavior at basin-scale river system because the changes in connectivity may lead to changes in morphodynamics and sediment budgets (Fryirs et al., 2007; Turnbull et al., 2008). Connectivity studies in different parts of the world, for example, India (Mishra et al., 2019; Swarnkar et al., 2020), China (Xie et al., 2020), Japan (López-Vicente et al., 2017), Spain (Llena et al., 2019), the Italian Alps (Cavalli et al., 2013; Martini et al., 2020), the Swiss Alps (Messenzehl et al., 2014), and Brazil (Zanandrea et al., 2019) shows how the connectivity at different scales (e.g., hillslope, river reach, sub-catchment) affect the sediment dynamics and geomorphic processes. Similarly, our connectivity analysis identified the upstream watershed as a sensitive part of the landscape where the channel network or the morphodynamics (e.g., hillslope-channel network, upslope erosion, activation of sediment source by landsliding) severely impacts the connectivity in downstream areas and hence the basin-wide fluvial-geomorphic processes.

The highly connected upstream region may increase the Brahmaputra's sediment flux, but the reduced connectivity downstream may cause sediment storage within the floodplain and contribute to the river bed aggradation (Fryirs et al., 2007; Poeppl et al., 2020). The partial connectivity or (dis)connectivity scenario observed here may form a barrier to sediment movement (transport-limited system), restraining the large volume of sediment transfer supplied from upstream along the lowland plain (Brierley and Fryirs, 2005; Fryirs and Brierley, 2013). The (dis)connectivity affects the internal dynamics of the sediment cascade both spatially and temporally, which provides a basis to examine cumulative responses to disturbance, whether natural or human-induced (Fryirs and Brierley, 2013). In partially connected or disconnected systems, materials eroded and transported from upstream parts of catchments may be deposited in accumulation zones (lowland plains or broad alluvial plains) over different periods, marked by alluviation, aggradation, and long-term sediment storage (Brierley and Fryirs, 2005; Jain and Tandon, 2010; Fryirs and Brierley, 2013). The sediment storage scenario (~49% of eroded sediments) and river bed aggradation rate (~1.47 cm/yr in the Brahmaputra) before the mouth of the Ganges–Brahmaputra (GB) rivers (Islam et al., 1999; Garzanti et al., 2011; Ashworth and Lewin, 2012, Dietrich et al., 2020; Faisal and Hayakawa, 2022), convincingly supports our study's observation, with the decreased connectivity or (dis)connectivity the depositional features may become prominent and hence may affect basin-wide geomorphic linkages.

Table 7. Comparison of the overall response to sediment connectivity

Basin	Remarks based on meteorology, geo-morphometry, topographic, and connectivity features
Teesta	Steep terrain, high relief ratio, higher SPI, STI, and IC at UPS, and higher annual rainfall infer a highly connected system, but dissected stream profiles and lower topographic control at MDS and DWS limit connectivity potentials.
Torsa	Steep terrain, high relief, higher SPI, STI, and IC values at UPS with moderate annual rainfall infer a highly connected system for potential sediment transportation. However, connectivity decreases at DWS caused by lower SPI and topographic control.
Manas	Moderate relief ratio, gentle stream profiles, and lower annual rainfall infers a moderately connected system instead of relatively higher IC values at UPS compare to MDS and DWS.

5. 3 Sediment transport potentials and implications

The sediment dynamics of these basins may be controlled by climatic, hydrological, geomorphometric, and sediment connectivity patterns. The SPI works as a proxy of discharge, which is related to the upslope contributing area and represents topographic steepness (Fontana and Marchi, 2003). Furthermore, Swarnkar et al. (2020) showed that sediment connectivity and stream power have equal importance in efficient sediment transport to the downstream region. Furthermore, the lower AIC value from the GLMMs test defines SPI as one of the influential factors on sediment connectivity potentials (Supplementary Table S1). Therefore, SPI and IC have been integrated to demonstrate the combined effects on these basins’ sediment transport potentials or accessibility. Then, the sediment transport potential maps (STPM) are prepared for respective basins (Fig. 11), which provides a general portrait of sediment transfer potentials and conveys critical information to identify the reaches that may receive higher sediment supply and transport along the main channel. The STPM raster images have been classified into five classes using natural breaks classification with successive classes of 'very low,' 'low,' 'average,' 'high,' and 'very high,' indicating increasing potential sediment transport (Xie et al., 2020). Our analysis suggests higher sediment transport potential along the UPS region. In contrast, the MDS and DWS regions have low to very low sediment transport potential and may favor sediment deposition. These depositional phenomena may increase the severity of hydrological floods and erosion in the downstream region. For instance, approximately 2000 km of river reaches of Bangladesh annually experience bank erosion because of the floods, which resulted in the increase of homeless or landless people or even loss of human life (28,700 and 600 deaths caused by the flood of 1974 and 2007, respectively) (Siddiqui et al., 2018; Mondal et al., 2020; Pradhan et al., 2021).

Hence, in the simplified representation of sediment transport potential maps, areas characterized by high to very high or low to very low value classes could become observation hotspots for future hydrological or sediment disaster management focusing downstream. For instance, identifying hot spot connectivity areas, strategic dredging or de-siltation of sediments, river interlinking, and improvements in channel navigation that consider the potential sediment transfer pathways and geomorphic processes can be effective for disaster management in the deltaic landscape of a downstream country in South Asia that is densely populated (about 41% of the basin's population of 83 million resides in Bangladesh) (Mahanta et al., 2014; Foerster et al., 2014; Wohl et al., 2019; Martini et al., 2019). Our study provides the sediment transport pathways, a prerequisite for an efficient sediment management framework (White and Apitz, 2008) and sustainable river basin management (World Bank, 2015), encouragingly practiced in neighboring countries like India (Mishra et al., 2019; Swarnkar at al., 2020), China (Xie et al., 2020; Jing et al., 2022), and other parts of the world (Poeppl et al., 2020). Moreover, the conceptual considerations gained with morphometric GIS approaches and field investigation provides a valuable representation of sediment dynamics and fluvial geomorphic processes, particularly at the basin scale. However, it should be mentioned that the current approach to representing potential sediment transfer does not consider the whole spectrum of the sediment transfer process, e.g., high runoff, precipitation events, monsoonal floods, landslides events, etc. Furthermore, sediment size exerts significant influence on the sediment transport and depositional processes in the river system, which is highly variable and requires extensive grain size analysis for a better representation of sediment runoff in these large basins (Fryirs and Brierley, 2013; Oyedotun, 2016). Addressing these issues requires a more sophisticated approach with increased input data (higher resolution multitemporal DEM, more ground-based observations, river discharge data, etc.). In addition, it should be noted that the sediment transport potential may be changed, reduced, or disconnected by various anthropogenic structures on the upstream channel for multiple purposes like hydroelectric power generation, irrigation, navigation, water supply, flood moderation, etc. (Pradhan et al., 2021). Therefore, river engineering structures like embankments, dams, barrages, etc., should be planned in such a sustainable way that does not disturb the hydro-geomorphic regime and, simultaneously, lower the risk of recurrent sediment disasters in downstream regions. In addition, the proposed workflow, which is developed from open-source data, can be replicated in other areas where the high-resolution data are not available or inaccessible, but large-scale sediment transport processes need to be investigated effectively.

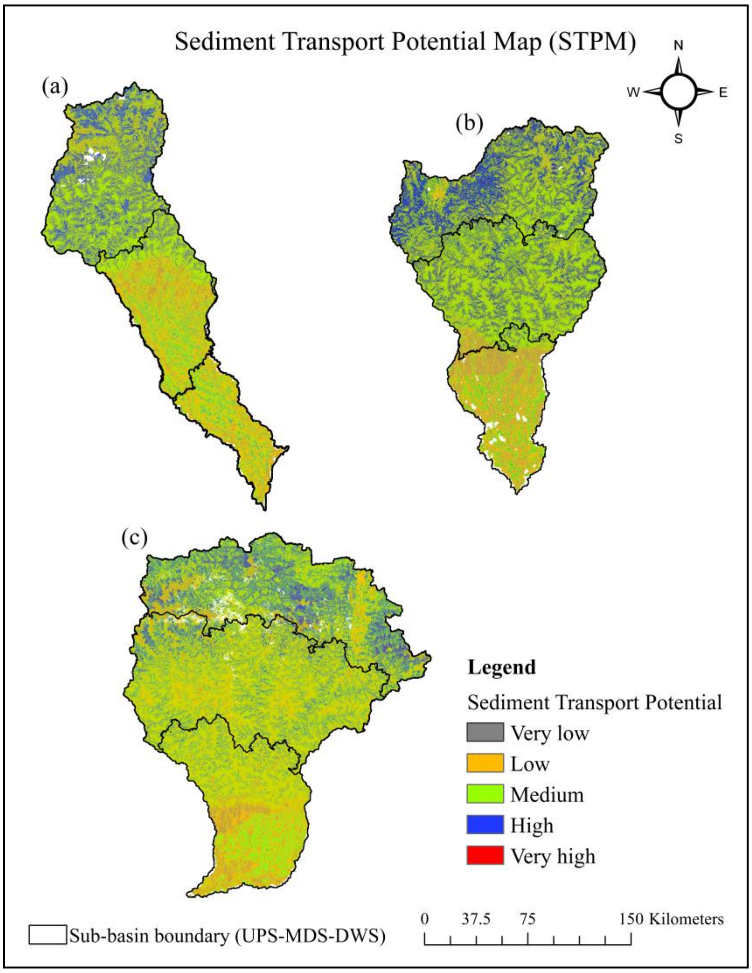

Fig. 11. Sediment transport potential maps for (a) Teesta, (b) Torsa, and (c) Manas basin.

6. Conclusions

The middle Brahmaputra River basin's geomorphic diversity and sediment connectivity have been studied using meteorological factors (rainfall and discharge variability), geomorphometric and topographic variables, and a sediment connectivity index. These basins are characterized by contrasting morphometry, steep and dissected channel profiles, different topographic responses, and inhomogeneous sediment connectivity patterns that affect the river system's overall connectivity and sediment transport potentials from upstream to downstream. The highly connected system at the upstream zone with steep topography and higher rainfall intensity demonstrates its higher sediment transport potential. Nevertheless, the connectivity reduces in the mid-to-downstream area with mild or low topographic features, lowering the sediment transport potential and resulting in deposition, which may affect the basin-wide geomorphic processes. Despite limitations in DEM resolution and functionalities of IC and topographic indices, the computation of IC and other topographic parameters from the present study in an understudied basin gives a general portrait of sediment transport behavior, providing the first step towards integrated river basin management. This study contributes to the current literature and would be helpful to local administrators or policymakers in future river adjustments and planning, where understanding sediment connectivity or sediment transport pathways is crucial for large-scale sediment management and integrated river basin management. Additionally, understanding large-scale sediment connectivity and its impacts on sediment transport because of monsoon dynamics, climate change scenarios, and human interventions in the upper Brahmaputra is the most challenging problem in such large basins, which needs to be investigated in the future. Therefore, the current approach of integrating the geomorphic characteristics, topographic features, and connectivity index from freely available remote sensing data and easily implementable geospatial tools may encourage different groups of researchers to carry out multi-temporal geomorphic analysis (event-based, monthly, seasonal and annual scale) taking this study result as baseline information for future investigations. Furthermore, the availability of high-resolution multi-temporal DEM and ground-based sediment yield observations can provide further insights into the factors controlling fluvial dynamics and sediment connectivity in such diverse transboundary river basins.

List of abbreviations

AIC: Akaike information criterion

ASCII: American standard code for information interchange

ASTER: Advanced spaceborne thermal emission and reflection radiometer

AW3D: ALOS global digital surface model

BWDB: Bangladesh water development board

DEM: Digital elevation model

DTM: Digital terrain model

ESA: European space agency

ESRI: Environmental system research institute inc.

GLAS: Geoscience laser altimeter system

GLMMs: Generalized linear mixed models

GRDC: Global runoff datacenter

GSI: Geospatial information authority of Japan

HAND: Height above the nearest drainage

IC: Connectivity index

ICESat-GLAS: Ice, cloud, and land elevation satellite-geoscience laser altimeter system

IMD: India meteorological department

IUCN: International union for conservation of nature and natural resources

JAXA: Japan aerospace exploration agency

LULC: Land-use/land-cover (LULC)

LPDAAC: Land processes distributed active archive center

LS: Slope-length

MEaSUREs: Making earth system data records for use in research environments

MERIT DEM: Multi-error-removed improved-terrain DEM

NASA: National aeronautics and space administration

NetCDF: Network common data form

PRISM: Panchromatic remote-sensing instrument for stereo mapping

SPI: Stream power index

SRTM: Shuttle radar topographic mission

STI: Sediment transport index

STPM: Sediment transport potential maps

TanDEM-X: TerraSAR-X add-on for digital elevation measurement

TauDEM: Terrain analysis using digital elevation models

TPI: Topographic position index

TRET: TRMM data extraction tool

TRMM: Tropical rainfall measuring mission

TWI: Topographic wetness index

Acknowledgements

This work was supported by the Ministry of Education, Culture, Sports, Science, and Technology (MEXT) scholarship. We are grateful to the editor Scott A. Lecce and two anonymous reviewers for their constructive comments and insightful suggestions, which immensely improved our manuscript.

References

Alam, S., Ali, M.M., Islam, Z., 2016. Future streamflow of Brahmaputra River Basin under synthetic climate change scenarios. J. Hydrol. Eng. 21(11), 05016027. https://doi.org/10.1061/(ASCE)HE.1943-5584.0001435

Alca´ntara-Ayala, I., 2002. Geomorphology, natural hazards, vulnerability and prevention of natural disasters in developing countries. Geomorphology 47 (2–4), 107–124. https://doi.org/10.1016/S0169-555X(02)00083-1

Akaike, H., 1974. A new look at the statistical model identification. IEEE Trans. Automat. Contr. 19 (6), 716–723. https://doi.org/10.1109/tac.1974.1100705

Alam, M.K., Negishi, J.N., Pongsivapai, P., Yamashita, S., Nakagawa, T., 2021. Additive effects of sediment and nutrient on leaf litter decomposition and macroinvertebrates in hyporheic zone. Water 13(10), 1340. https://doi.org/10.3390/w13101340

Allison, M.A., Kuehl, S.A., Martin, T.C., Hassan, A., 1998. Importance of flood-plain sedimentation for river sediment budgets and terrigenous input to the oceans: insights from the Brahmaputra–Jamuna River. Geology 26(2), 175–178. https://doi.org/10.1130/0091-7613(1998)026%3C0175:IOFPSF%3E2.3.CO;2

Amatulli, G., McInerney, D., Sethi, T., Strobl, P., Domisch, S., 2020. Geomorpho90m-global high-resolution geomorphometry layers. Sci. Data 7, 162. https://doi.org/10.1038/s41597-020-0479-6

Arabameri, A., Pradhan, B., Pourghasemi, H.R., Rezaei, K., Kerle, N., 2018. Spatial modelling of gully Erosion using GIS and R programing: A comparison among three data mining algorithms. Appl. Sci. 8(8), 1369. https://doi.org/10.3390/app8081369

Arabkhedri, M., Heidary, K., Parsamehr, M.R., 2021. Relationship of sediment yield to connectivity index in small watersheds with similar erosion potentials. J. Soils Sediments 21, 2699–2708. https://doi.org/10.1007/s11368-021-02978-z

Arulbalaji, P., Gurugnanam, B., 2017. Geospatial tool-based morphometric analysis using SRTM data in Sarabanga watershed, Cauvery River, Salem district, Tamil Nadu, India. Appl. Water Sci. 7 (7), 3875–3883. https://doi.org/10.1007/s13201-017-0539-z

Ashworth, P.J., Lewin, J., 2012. How do big rivers come to be different? Earth Sci. Rev. 114 (1–2a), 84–107. https://doi.org/10.1016/j.earscirev.2012.05.003

Baartman, J.E.M., Masselink, R., Temme, A.J.A.M., Keesstra, S.D., 2013. Linking landscape morphological complexity and sediment connectivity. Earth Surf. Proc. Land. 38(12), 1457–1471. https://doi.org/10.1002/esp.3434

Bajracharya, S.R., Palash, W., Shrestha, S., Khadgi, V.R., Duo, C., Das, P.J, Dorji, C., 2015. Systematic evaluation of satellite-based rainfall products over the Brahmaputra basin for hydrological applications. Adv. Meteorol. 398687. https://doi.org/10.1155/2015/398687

Bandyopadhyay, S., Das, S., SekharKar, N., 2021. Avulsion of the Brahmaputra in Bangladesh during the 18th–19th Century: a review based on cartographic and literary evidence. Geomorphology 384, 107696. https://doi.org/10.1016/j.geomorph.2021.107696

Bandyopadhyay, S., Kar, N.S., Dasgupta, S., Mukherjee, D., Das, A., 2023. Island area changes in the Sundarban region of the abandoned western Ganga–Brahmaputra–Meghna Delta, India and Bangladesh. Geomorphology 422, 108482. https://doi.org/10.1016/j.geomorph.2022.108482

Bhatt, S., Ahmed, S.A., 2014. Morphometric analysis to determine floods in the Upper Krishna basin using Cartosat DEM. Geocarto Int. 29(8), 878–894. https://doi.org/10.1080/10106049.2013.868042

Bindu, G., Neelkantan, R., Ragunath, R., 2012. Assessment of morphometric characteristics of Chittar river basin, Triruvantpuram district, Kerala: a remote sensing and GIS based study. J. Indian Geomorphology 1, 127–132.

Borselli, L., Cassi, P., Torri, D., 2008. Prolegomena to sediment and flow connectivity in the landscape: a GIS and field numerical assessment. Catena 75(3), 268–277. https://doi.org/10.1016/j.catena.2008.07.006

Brierley, G.J., Fryirs, K.A., 2005. Geomorphology and River Management: Applications of the River Styles Framework. Blackwell Publications, Oxford, UK. https://doi.org/10.1002/9780470751367

Brierley, G., Fryirs, K., Jain, V., 2006. Landscape connectivity: the geographic basis of geomorphic applications. Area 38, 165–174. https://doi.org/10.1111/j.1475-4762.2006.00671.x

Bracken, L.J., Turnbull, L., Wainwright, J., Bogaart, P., 2015. Sediment connectivity: a framework for understanding sediment transfer at multiple scales. Earth Surf. Proc. Land. 40, 177–188. https://doi.org/10.1002/esp.3635

Brahmaputra Board, 1995. Additional Volume for Master Plan of Brahmaputra basin, Part-1: Main stem, Published by Brahmaputra Board, India.

Brammer, H., 2014. Bangladesh's dynamic coastal regions and sea-level rise. Clim. Risk Manag. 1, 51–62. https://doi.org/10.1016/j.crm.2013.10.001

Buckley, S.M, Agram, P.S., Belz, J.E., Crippen, R.E., Gurrola, E.M., Hensley, S., Kobrick, M., Lavalle, M., Martin, J.M., Neumann, M., Nguyen, Q.D., Rosen, P. A., Shimada, J.G., Simard, M., Tung, W.W., 2020. NASA-DEM user guide. NASA Jet Propulsion Laboratory, January, California, USA. https://lpdaac.usgs.gov/documents/1318/NASADEM_User_Guide_V12.pdf (accessed on 15 March 2021)

Burrough, P.A., McDonnell, R., McDonnell, R.A., Lloyd, C.D., 2015. Principles of Geographical Information Systems. Oxford university press, UK.

Buter, A., Heckmann, T., Filisetti, L., Savi, S., Mao, L., Gems, B., Comiti, F., 2022. Effects of catchment characteristics and hydro-meteorological scenarios on sediment connectivity in glacierised catchments. Geomorphology 402, 108128. https://doi.org/10.1016/j.geomorph.2022.108128

Cantreul, V., Bielders, C., Calsamiglia, A., Degré, A., 2018. How pixel size affects a sediment connectivity index in central Belgium. Earth Surf. Proc. Land. 43(4), 884–893. https://doi.org/10.1002/esp.4295

Cavalli, M., Marchi, L., 2008. Characterization of the surface morphology of an alpine alluvial fan using airborne LiDAR. Nat. Hazards Earth Syst. Sci. 8, 323–333. https://doi.org/10.5194/nhess-8-323-2008

Cavalli, M., Trevisani, S., Comiti, F., Marchi, L., 2013. Geomorphometric assessment of spatial sediment connectivity in small Alpine catchments. Geomorphology 188, 31–41. https://doi.org/10.1016/j.geomorph.2012.05.007

Cavalli, M., Crema, S., Marchi, L., 2014. Guidelines on the sediment connectivity ArcGIS toolbox and stand-alone application (no Release 1.0, Issue June), 1–33. http://dx.doi.org/10.13140/RG.2.1.3243.5361

Chauniyal, D.D., Dutta, S., 2018. Application of topographic position index for classification of landforms in Dudhatoli region of Garhwal Himalaya, Uttarakhand. J. Indian Geomorphol. 6, 28–41.

Chen, C.Y., Yu, F.C., 2011. Morphometric analysis of debris flows and their source areas using GIS. Geomorphology 129, 387–397. https://doi.org/10.1016/j.geomorph.2011.03.002

Cheng, N.N., He, H.M., Yang, S.Y., Lu, Y.J., Jing, Z.W., 2017. Impacts of topography on sediment discharge in Loess Plateau, China. Quat. Int. 440, 119–129. https://doi.org/10.1016/j.quaint.2016.12.005

Cho, H., 2020. A recursive algorithm for calculating the longest flow path and its iterative implementation. Environ. Model. Soft. 131, 104774. https://doi.org/10.1016/j.envsoft.2020.104774

Clarke, J.I., 1966. Morphometry from maps. In: G.H. Dury (Editor), Essays in Geomorphology. Heinemann, London, pp. 235–274.

Clubb, F.J., Mudd, S.M., Attal, M., Milodowski, D.T, Grieve, S.W.D., 2016. The relationship between drainage density, erosion rate, and hilltop curvature: Implications for sediment transport processes. J. Geophys. Res. Earth Surf. 121(10), 1724–1745. https://doi.org/10.1002/2015JF003747

Coleman, J.M., 1969. Brahmaputra River: channel processes and sedimentation. Sediment. Geol. 3, 129–239. https://doi.org/10.1016/0037-0738(69)90010-4

Crema, S., Cavalli, M., 2018. SedInConnect: a stand-alone, free and open source tool for the assessment of sediment connectivity. Comput. Geosci. 111, 39–45. https://doi.org/10.1016/j.cageo.2017.10.009

Crippen, R., Buckley, S., Belz, E., Gurrola, E., Hensley, S., Kobrick. M., Lavalle, M., Martin, J., Neumann, M., Nguyen, Q., 2016. NASADEM global elevation model: methods and progress. Int. Arch. Photogramm. Remote Sens. Spatial Inf. Sci. XLI-B4, 125–128. https://doi.org/10.5194/isprs-archives-XLI-B4-125-2016

Das, S., Bora, P.K., Das, R., 2022. Estimation of slope length gradient (LS) factor for the sub-watershed areas of Juri River in Tripura. Model. Earth Syst. Environ. 8, 1171–1177. https://doi.org/10.1007/s40808-021-01153-0

Debelo, G., Tadele, K., Korich, S.A., 2017. Morphometric analysis to identify erosion prone areas on the upper blue Nile using GIS: case study of Didessa and Jema sub- basin, Ethiopia. Int. Res. J. Eng. Technol. 04 (08), 1773–1784.

De Reu, J., Bourgeois, J., Bats, M., Zwertvaegher, A., Gelorini, V., De Smedt, P., Chu, W., Antrop, M., De Maeyer, P., Finke, P., Van Meirvenne, M., Verniers, J., Crombé, P., 2013. Application of the topographic position index to heterogeneous landscapes. Geomorphology 186, 39–49. https://doi.org/10.1016/j.geomorph.2012.12.015

De Roo, A.P.J., 1998. Modelling runoff and sediment transport in catchments using GIS. Hydrol. Process. 12, 905–922. https://doi.org/10.1002/(SICI)1099-1085(199805)12:6%3C905::AID-HYP662%3E3.0.CO;2-2

Dewan, A., Corner, R., Saleem, A., Rahman, M.M., Haider, M.R., Rahman, M.M., Sarker, M.H., 2017. Assessing channel changes of the Ganges–Padma River system in Bangladesh using Landsat and hydrological data. Geomorphology 276, 257–279. https://doi.org/10.1016/j.geomorph.2016.10.017

Dietrich, M., Best, K.B., Raf, J.L., Ronay, E.R., 2020. A first-order geochemical budget for suspended sediment discharge to the Bay of Bengal from the Ganges–Brahmaputra river system. Sci. Total Environ. 726, 66. https://doi.org/10.1016/j.scitotenv.2020.138667

Dormann, C.F., Elith, J., Bacher, S., Buchmann, C., Carl, G., Carré, G., Marquéz, J.R.G., Gruber, B., Lafourcade, B., Leitão, P.J., Münkemüller, T., Mcclean, C., Osborne, P.E., Reineking, B., Schröder, B., Skidmore, A.K., Zurell, D., Lautenbach, S., 2013. Collinearity: A review of methods to deal with it and a simulation study evaluating their performance. Ecography 36(1), 27–46. https://doi.org/10.1111/j.1600-0587.2012.07348.x

Faghih, A., Nourbakhsh, A., Kusky, T.M., 2015. GIS-Based analysis of relative tectonic activity along the Kazerun Fault Zone, Zagros Mountains, Iran, insights from data mining of geomorphic data. J. Earth Sci. 26, 712–723. https://doi.org/10.1007/s12583-015-0583-2

Faisal, B.M.R., Hayakawa, Y.S., 2022. Geomorphological processes and their connectivity in hillslope, fluvial, and coastal areas in Bangladesh: A review. Prog. Earth Planet. Sci. 9, 41. https://doi.org/10.1186/s40645-022-00500-8

FAO, 1978. Methodology for assessing soil degradation. Report on the FAO/UNEP expert consultation, Rome.

Fontana, G.D., Marchi, L., 1998. GIS Indicators for Sediment Sources Study in Alpine Basins. In: Kovar, K., Tappeiner, U., Peters, N.E., Craig, R.G., (Eds.), Hydrology, Water Resources and Ecology in Headwaters. IAHS Publication 248, International Association of Hydrological Sciences: Wallingford. pp. 553–560.

Fontana, G.D., Marchi. L., 2003. Slope-area relationships and sediment dynamics in two alpine streams. Hydrol. Process. 17(1), 73–87. https://doi.org/10.1002/hyp.1115

Foster, G. R., 1990. Process based modelling of soil erosion by water on agricultural land [M]. In: Boardman, J., Foster I.D.L., Dearing, J.A. (Eds.), British Geomorphological Research Group symposium series: soil erosion on agricultural land. Chichester, Wiley, pp. 429–445.

Foerster, S., Wilczok, C., Brosinsky, A., Segl, K., 2014. Assessment of sediment connectivity from vegetation cover and topography using remotely sensed data in a dryland catchment in the Spanish Pyrenees. J. Soils Sediments 14 (12), 1982–2000. https://doi.org/10.1007/s11368-014-0992-3

Franks, S., Storey, J., Rengarajan, R., 2020. The new Landsat collection-2 digital elevation model. Remote Sens. 12(23), 3909. https://doi.org/10.3390/rs12233909

Fryirs, K.A., Brierley, G.J., Preston, N.J., Kasai, M., 2007. Buffers, barriers and blankets: the (dis)connectivity of catchment-scale sediment cascades. Catena 70, 49–67. https://doi.org/10.1016/j.catena.2006.07.007

Fryirs, K.A., Brierley, G.J., 2013. Geomorphic Analysis of River Systems: An approach to Reading the Landscape. John Wiley and Sons, Chichester. https://doi.org/10.1002/9781118305454

Gallant, J.C., Wilson, J.P., 2000. Primary topographic attributes. In: Wilson, J.P., Gallant, J.C. (Eds.), Terrain Analysis: Principles and Applications. Wiley, New York. pp. 51–85.

Gallant, J. C., Dowling, T. I., 2003. A multiresolution index of valley bottom flatness for mapping depositional areas, Water Resour. Res. 39, 1347, https://doi.org/10.1029/2002WR001426

García Rodriguez, J.L., Giménez Suarez, M.C., 2010. Historical review of topographic factor of LS, of water erosion models. Aqua- LAC 2, 56–61. https://unesdoc.unesco.org/ark:/48223/pf0000211564

Ganasri, B.P., Ramesh, H., 2016. Assessment of soil erosion by RUSLE model using remote sensing and GIS-A case study of Nethravathi Basin. Geosci. Front. 7(6), 953-961. https://doi.org/10.1016/j.gsf.2015.10.007

Goodbred, S.L., Paolo, P.M., Ullah, M.S., Pate, R.D., Khan, S.R., Kuehl, S.A., Rahaman, W., 2014. Piecing together the Ganges-Brahmaputra-Meghna River delta: Use of sediment provenance to reconstruct the history and interaction of multiple fluvial systems during Holocene delta evolution. Geol. Soc. Am. Bull. 126 (11-12), 1495–1510. https://doi.org/10.1130/B30965.1

Goswami, D.C., 1985. Brahmaputra River, Assam, India: physiography, basin denudation, and channel aggradation. Water Resour. Res. 21(7), 959–978. https://doi.org/10.1029/WR021i007p00959

Goswami, D.C., 1998. Fluvial Regime and Flood Hydrology of the Brahmaputra River, Assam. In: Kale, V.S. (Eds.), Flood Studies in India. Bangalore: Geological Society of India, Memoir. 41, pp. 53–76.

Goyal, M.K., Goswami, U.P., 2018. Teesta River and its Ecosystem. In: Singh, D.S. (Eds.), The Indian Rivers. Springer Hydrogeology, Springer Nature Singapore Pte Ltd., pp. 537–551. https://doi.org/10.1007/978-981-10-2984-4_37

Grabs, T., Seibert, J., Bishop, K., Laudon, H., 2009. Modeling spatial patterns of saturated areas: A comparison of the topographic wetness index and a dynamic distributed model. J. Hydrol. 373, 15–23. https://doi.org/10.1016/j.jhydrol.2009.03.031

Garzanti, E., Vezzoli, G., Ando, S., France-lanord, C., Singh, S.K., Foster, G., 2004. Sand petrology and focused erosion in collision orogens: the Brahmaputra case. Earth Planet. Sci. Lett. 220, 157–174. https://doi.org/10.1016/S0012-821X(04)00035-4

Garzanti, E., Andó, S., France-Lanord, C., Censi, P., Vignola, P., Galy, V., Lupker, M., 2011. Mineralogical and chemical variability of fluvial sediments 2. Suspended-load silt

(Ganga–Brahmaputra, Bangladesh). Earth Planet. Sci. Lett. 302 (1–2), 107–120. https://doi.org/10.1016/j.epsl.2010.11.043

Gravelius, H., 1914. Grundrifi der gesamten Gewcisserkunde. Band I: Flufikunde (Compendium of Hydrology, Vol. I. Rivers, in German). Goschen, Berlin.

GRDC, 2021. Discharge data obtained from the Global Runoff Data Centre. Koblenz, Germany-Federal Institute of Hydrology (BfG). https://www.bafg.de/GRDC/EN/01_GRDC/grdc_node.html (accessed on Jan 2021)

Grohmann, C.H., Riccomini, C., 2009. Comparison of roving-window and search-window techniques for characterising landscape morphometry. Comput. Geosci. 35, 2164–2169. https://doi.org/10.1016/j.cageo.2008.12.014

Gupta, H., Kao, S., Dai, M., 2012. The role of mega dams in reducing sediment fluxes: A case study of large Asian rivers. J. Hydrol. 464–465. https://doi.org/10.1016/j.jhydrol.2012.07.038

Hadley, R.F., Schumm, S.A., 1961. Sediment sources and drainage basin characteristics in upper Cheyenne River basin. US Geological Survey Water- Supply Paper 1531- B, 198. https://doi.org/10.3133/wsp1531

Hayakawa, Y.S., Oguchi, T., 2006. DEM-based identification of fluvial knickzones and its application to Japanese mountain rivers. Geomorphology 78(1), 90–106. https://doi.org/10.1016/j.geomorph.2006.01.018

Heine, R.A., Lant, C.L., Sengupta, R.R., 2004. Development and comparison of approaches for automated mapping of stream channel networks. Ann. Am. Assoc. Geogr. 94, 477–490. https://doi.org/10.1111/j.1467-8306.2004.00409.x

Heckmann, T., Cavalli, M., Cerdan, O., Foerster, S., Javaux, M., Lode, E., Smetanova, A., Vericat, D., Brardinoni, F., 2018. Indices of sediment connectivity: opportunities, challenges and limitations. Earth Sci. Rev. 187, 77–108. https://doi.org/10.1016/j.earscirev.2018.08.004

Higgins, S. A., Overeem, I., Rogers, K.G., Kalina, E. A., 2018. River linking in India: Downstream impacts on water discharge and suspended sediment transport to deltas. Elem. Sci. Anth. 6, 20. https://doi.org/10.1525/elementa.269

Horton, R. E., 1932. Drainage basin characteristics. Trans. Am. Geophys. Union 13, 350–361. http://dx.doi.org/10.1029/TR013i001p00350

Horton, R. E., 1945. Erosional development of streams and their drainage basins; hydro-physical approach to quantitative morphology. Geol. Soc. Am. Bull. 56, 275–370. https://doi.org/10.1130/0016-7606(1945)56[275:EDOSAT]2.0.CO;2

Hu, P., Gao, X., Mu, G., Zhao, W., Sun, P., Li, L., 2019. Runoff-sediment dynamics under different flood patterns in a Loess Plateau catchment, China. Catena 173, 234–245. https://doi.org/10.1016/j.catena.2018.10.023

Huffman, G. J., Bolvin, D. T., Nelkin, E. J., Wolff, D.B., Adler, R.F., Gu, G., Stocker, E.F., 2007. The TRMM Multisatellite Precipitation Analysis (TMPA): Quasi-global, multiyear, combined-sensor precipitation estimates at fine scales. J. Hydrometeorol. 8(1), 38–55. https://doi.org/10.1175/JHM560.1

Huffman, G.J., Adler, R.F., Bolvin, D.T., Nelkin, E.J., 2010. The TRMM Multisatellite Precipitation Analysis (TMPA) Chapter 1. In: Hossain, F., Gebremichael, M., (Eds.), Satellite Rainfall Applications for Surface Hydrology, Springer Verlag, Berlin, pp. 3–22. https://doi.org/10.1007/978-90-481-2915-7_1

Hungr, O., Morgan, G.C., Kellerhals, P., 1984. Quantitative analysis of debris hazards for design of remedial measures. Can. Geotech. J. 21, 663–677. https://doi.org/10.1139/t84-073

Immerzeel, W., 2008. Historical trends and future predictions of climate variability in the Brahmaputra Basin. Int. J. Climatol. 28(2), 243–254. https://doi.org/10.1002/joc.1528

Islam, M.R., Begum, S.F., Yamaguchi, Y., Ogawa, K., 1999. The Ganges and Brahmaputra Rivers in Bangladesh: basin denudation and sedimentation. Hydrol. Process. 17, 2907–2923. https://doi.org/10.1002/(SICI)1099-1085(19991215)13:17%3C2907::AID-HYP906%3E3.0.CO;2-E

Iqbal, J., Read, J.J., Thomasson, A.J., Jenkins, J.N., 2005. Relationships between soil landscape and dryland cotton lint yield. Soil Sci. Soc. Am. J. 69, 872–882. https://doi.org/10.2136/sssaj2004.0178

Iwahashi, J., Yamazaki, D., Nakano, T., Endo, R., 2021. Classification of topography for ground vulnerability assessment of alluvial plains and mountains of Japan using 30 m DEM. Prog. Earth Planet. Sci. 8, 3. https://doi.org/10.1186/s40645-020-00398-0

Iwahashi, J., Yamazaki, D., 2022. Global polygons for terrain classification divided into uniform slopes and basins. Prog. Earth Planet. Sci. 9, 33. https://doi.org/10.1186/s40645-022-00487-2

Jain, V., Tandon, S.K., Sinha, R., 2012. Application of modern geomorphic concepts for understanding the spatio-temporal complexity of the large Ganga river dispersal system. Curr. Sci. 103(11), 1300–1319. http://www.jstor.org/stable/24089150

Jain, V., Tandon, S.K., 2010. Conceptual assessment of (dis) connectivity and its application to the Ganga River dispersal system. Geomorphology 118 (3–4), 349–358. https://doi.org/10.1016/j.geomorph.2010.02.002

Jenson, S.K., Domingue, J.O., 1988. Extracting topographic structure from digital elevation data for geographic information system analysis. Photogramm. Eng. Remote Sens. 54(1), 593–600.

Jiang, W., Han, Z., Zhang, J., Jiao, Q., 2016. Stream profile analysis, tectonic geomorphology and neotectonic activity of the Damxung-Yangbajain rift in the south Tibetan Plateau. Earth Surf. Process. Landforms 41(10), 1312–1326. https://doi.org/10.1002/esp.3899

Jing, Y., Zhao, Q., Lu, M., Wang, A., Yu, J., Liu, Y., Ding, S., 2022. Effects of road and river networks on sediment connectivity in mountainous watersheds. Sci. Total Environ. 826, 154189. https://doi.org/10.1016/j.scitotenv.2022.154189

Jourgholami, M., Karami, S., Tavankar, F., Lo Monaco, A., Picchio, R., 2021. Effects of slope gradient on runoff and sediment yield on machine-induced compacted soil in temperate forests. Forests 12 (1), 49. https://doi.org/10.3390/f12010049

Kalantari, Z., Nickman, A., Lyon, S.W., Olofsson, B., Folkeson, L., 2014. A method for mapping flood hazard along roads. J. Environ. Manage. 133, 69–77. https://doi.org/10.1016/j.jenvman.2013.11.032

Kale, V.S., 2003. Geomorphic effects of monsoon floods on Indian rivers. Nat. Hazards 28, 65–84. https://doi.org/10.1023/A:1021121815395

Kale, V.S., 2005. Fluvial hydrology and geomorphology of monsoon dominated Indian rivers. Rev. Bras. de Geomorfol. 6(1), 63–73. https://doi.org/10.20502/rbg.v6i1.39

Kanhaiya, S., Singh, B.P., Singh, S., Mittal, P., Srivastava, V.K., 2018. Morphometric analysis, bedload sediments, and weathering intensity in the Khurar River Basin, central India. Geol. J. 54(1), 466–481. https://doi.org/10.1002/gj.3194

Karra, K., Kontgis, C., Statman-Weil, Z., Mazzariello, J.C., Mathis, M.M., Brumby, S.P., 2021. Global land use / land cover with Sentinel 2 and deep learning. 2021 IEEE International Geoscience and Remote Sensing Symposium IGARSS, Brussels, Belgium. pp. 4704–4707. https://doi.org/10.1109/IGARSS47720.2021.9553499

Kaushal, R.K., Sarkar, A., Mishra, K., Sinha, R., Nepal, S., Jain, V., 2020. Spatio-temporal variability in stream power distribution in the Upper Kosi River basin, Central

Himalaya: Controls and geomorphic implications. Geomorphology 350, 106888. https://doi.org/10.1016/j.geomorph.2019.106888

Khan, M.S.S., Islam, A.R.M.T., 2015. Anthropogenic impact on morphology of Teesta river in northern Bangladesh: An exploratory study. Int. J. Geomat. Geosci. 3(3), 50–55. http://pubs.sciepub.com/jgg/3/3/1

Lane, S.N., Richards, K.S., 1997. Linking river channel form and process: time, space and causality revisited. Earth Surf. Process. Landforms 22, 249–260. https://doi.org/10.1002/(SICI)1096-9837(199703)22:3%3C249::AID-ESP752%3E3.0.CO;2-7

Li, J., Zhao, Y., Bates, P., Neal, J., Tooth, S., Hawker, L., Maffei, C., 2020. Digital Elevation Models for topographic characterization and flood flow modelling along low-gradient, terminal dryland rivers-A comparison of space borne datasets for the Río Colorado, Bolivia. J. Hydrol. 591, 125617. https://doi.org/10.1016/j.jhydrol.2020.125617

Liu, W., Shi, C., Ma, Y., Li, H., Ma, X., 2021. Land use and land cover change-induced changes of sediment connectivity and their effects on sediment yield in a catchment on the Loess Plateau in China. Catena 207 (11), 105688. https://doi.org/10.1016/j.catena.2021.105688

Li, Z., Chen, J., Tan, C., Zhou, X., Li, Y., Han, M., 2021. Debris flow susceptibility assessment based on topo-hydrological factors at different unit scales: a case study of Mentougou district, Beijing. Environ. Earth Sci. 80, 365. https://doi.org/10.1007/s12665-021-09665-9

Li, H., Zhao, J., Yan, B., Yue, L., Wang, L., 2022. Global DEMs vary from one to another: an evaluation of newly released Copernicus, NASA and AW3D30 DEM on selected terrains of China using ICESat-2 altimetry data. Int. J. Digit. Earth 15 (1), 1149–1168. https://doi.org/10.1080/17538947.2022.2094002

Llena, M., Vericat, D., Cavalli, M., Crema, S., Smith, M.W., 2019. The effects of land use and topographic changes on sediment connectivity in mountain catchments. Sci. Total Environ. 660, 899–912. https://doi.org/10.1016/j.scitotenv.2018.12.479

López-Vicente, M., Poesen, J., Navas, A., Gaspar, L., 2013. Predicting runoff and sediment connectivity and soil erosion by water for different land use scenarios in the Spanish Pre-Pyrenees. Catena 102, 62–73. https://doi.org/10.1016/j.catena.2011.01.001

López-Vicente, M., Sun, X., Onda, Y., Kato, H., Gomi, T., Hiraoka, M., 2017. Effect of tree thinning and skidding trails on hydrological connectivity in two Japanese forest catchments. Geomorphology 292, 104–114. https://doi.org/10.1016/j.geomorph.2017.05.006

Mahala, A., 2020. The significance of morphometric analysis to understand the hydrological and morphological characteristics in two different morpho-climatic settings. Appl. Water Sci. 10, 33. https://doi.org/10.1007/s13201-019-1118-2

Mahanta, C., Zaman, A. M., Newaz, S. M. S., Rahman, S. M., Mazumdar, T. K., Choudhury, R., Borah, P. J. Saikia, L., 2014. Physical Assessment of the Brahmaputra River. IUCN, International Union for Conservation of Nature, Dhaka, Bangladesh, pp xii + 74. https://portals.iucn.org/library/sites/library/files/documents/2014-083.pdf (accessed on 15 March 2021)

Martini, L., Picco, L., Iroumé, A., Cavalli, M., 2019. Sediment connectivity changes in an Andean catchment affected by volcanic eruption. Sci. Total Environ. 692, 1209–1222. https://doi.org/10.1016/j.scitotenv.2019.07.303

Martini, L., Faes, L., Picco. L., Iroumé, A., Lingua, E., Garbarino, M., Cavalli, M., 2020. Assessing the effect of fire severity on sediment connectivity in central Chile. Sci. Total Environ. 728, 139006. https://doi.org/10.1016/j.scitotenv.2020.139006

Medhioub, E., Bouaziz, M., Achour, H., Bouaziz, S., 2019. Monthly assessment of TRMM 3B43 rainfall data with high-density gauge stations over Tunisia. Arab. J. Geosci. 12(2), 1–14. https://doi.org/10.1007/s12517-018-4155-5

Messenzehl, K., Hoffmann, T., Dikau, R., 2014. Sediment connectivity in the high-alpine valley of Val Müschauns, Swiss National Park-linking geomorphic field mapping with geomorphometric modelling. Geomorphology 221, 215–229. https://doi.org/10.1016/j.geomorph.2014.05.033

Miller, J.C., 1953. A quantitative geomorphic study of drainage basin characteristics in the Clinch mountain area, Virginia and Tennessee. Technical report 3, Department of Geology, Columbia University, New York, pp. 389–402.

Mishra, K., Sinha, R., Jain, V., Nepal, S., Uddin, K., 2019. Towards the assessment of sediment connectivity in a large Himalayan river basin. Sci. Total Environ. 661, 251–265. https://doi.org/10.1016/j.scitotenv.2019.01.118

Mojaddadi, H., Pradhan, B., Nampak, H., Ahmad, N., Ghazali, A.H.B., 2017. Ensemble machine-learning-based geospatial approach for flood risk assessment using multi-sensor remote-sensing data and GIS. Geomat. Nat. Hazards Risk 8(2), 1080–1102. https://doi.org/10.1080/19475705.2017.1294113

Montgomery, D., Dietrich, W.E., 1989. Channel initiation, drainage density and slope. Water Resour. Res. 25, 1907–1918. https://doi.org/10.1029/WR025i008p01907

Mondal, M.S.H., Murayama, T., Nishikizawa, S., 2020. Assessing the flood risk of riverine households: A case study from the right bank of the Teesta River, Bangladesh. Int. J. Disaster Risk Reduct. 51, 101758. https://doi.org/10.1016/j.ijdrr.2020.101758

Mondal, M.S.H., Islam, M.S., 2017. Chronological trends in maximum and minimum water flows of the Teesta River, Bangladesh, and its implications. Jamba: J. Disaster Risk Stud. 9(1), a373. https://doi.org/10.4102/jamba.v9i1.373

Moore, I.D., Grayson, R., Ladson, A., 1991. Digital terrain modelling: a review of hydrological, geomorphological, and biological applications. Hydrol. Process. 5(1), 3–30. https://doi.org/10.1002/hyp.3360050103

Moore, I.D., Gesseler, P.E., Nielsen, G.A., Peterson, G.A., 1993. Soil attribute prediction using terrain analysis. Soil Sci. Soc. Am. J. 57, 443–452. https://doi.org/10.2136/sssaj1993.03615995005700020026x

Moore, I.D, Burch, G.J., 1986. Physical basis of the length-slope factor in the universal soil loss equation. Soil Sci. Soc. Am. J. 50, 1294–1298. https://doi.org/10.2136/sssaj1986.03615995005000050042x

Morgan, R.P.C., 2009. Soil erosion and conservation. John Wiley and Sons, Hoboken.

Najafi, S., Dragovich, D., Heckmann, T., Sadeghi, S.H., 2021. Sediment connectivity concepts and approaches. Catena 196, 104880. https://doi.org/10.1016/j.catena.2020.104880

NASA JPL, 2020. NASADEM Merged DEM Global 1 arc second V001 [Data set]. NASA EOSDIS Land Processes DAAC. https://doi.org/10.5067/MEaSUREs/NASADEM/NASADEM_HGT.001 (accessed on 11 May 2021)

NASA, 2017. README document for the Tropical Rainfall Measurement Mission (TRMM). Goddard Earth Sciences Data and Information Services Center (GES DISC). https://disc2.gesdisc.eosdis.nasa.gov/data/TRMM_L3/TRMM_3B43/doc/README.TRMM_V7.pdf (accessed on 15 June 2021)

Nepal, S., Flügel, W.A., Shrestha, A.B., 2014. Upstream-downstream linkages of hydrological processes in the Himalayan region. Ecol. Process 3, 19. https://doi.org/10.1186/s13717-014-0019-4

O'Callaghan, J. F., Mark, D. M., 1984. The extraction of drainage networks from digital elevation data. Comput. Graph. Image Process. 28, 328–344. http://dx.doi.org/10.1016/S0734-189X(84)80011-0

Oyedotun, T.D.T., 2016. Sediment characterisation in an Estuary-beach system. J. Coast. Zone Manag. 19(2), 433. Doi:10.4172/2473-3350.1000433

Oyedotun, T.D.T., 2020. Quantitative assessment of the drainage morphometric characteristics of Chaohu Lake Basin from SRTM DEM Data: a GIS-based approach. Geol. Ecol. Landsc. 6(3), 174–187. https://doi.org/10.1080/24749508.2020.1812147

Oguchi, T., Wasklewicz, T., Hayakawa, Y.S., 2013. Remote data in fluvial geomorphology: characteristics and applications. In: Shroder, J. (Editor in Chief), Wohl, E. (Ed.), Treatise on Geomorphology. Academic Press, San Diego, CA. Fluvial Geomorphology 9, pp. 711–729. https://doi.org/10.1016/B978-0-12-374739-6.00262-1

Oguchi, T., Hayakawa, Y.S., Wasklewicz, T., 2022. 6.50-Remote Data in Fluvial Geomorphology: Characteristics and Applications. In: John (Jack) F. Shroder Editor(s), Treatise on Geomorphology (Second Edition), Academic Press. pp. 1116–1142. https://doi.org/10.1016/B978-0-12-818234-5.00103-6

Ozdemir, H., Bird, D., 2009. Evaluation of morphometric parameters of drainage networks derived from topographic maps and DEM in point of floods. Environ Geol. 56(7), 1405–1415. https://doi.org/10.1007/s00254-008-1235-y

Ozulu, İ., Gökgöz, T., 2018. Examining the stream threshold approaches used in hydrologic analysis. ISPRS Int. J. Geo-Inf. 7(6), 201. https://doi.org/10.3390/ijgi7060201

Panagos, P., Borrelli, P., Meusburger, K., 2015. A new European slope length and steepness factor (LS-Factor) for modeling soil erosion by water. Geosciences 5(2), 117–126. https://doi.org/10.3390/geosciences5020117

Pangare, G., Nishat, B., Liao, X., Qaddumi, H.M., 2021. The Restless River. World Bank, Washington, DC. https://doi.org/10.1596/36258 (accessed on March 2022)

Pant, N., Dubey, R.K., Bhatt, A., Rai, S.P., Semwal, P., Mishra, S., 2020. Soil erosion and flood hazard zonation using morphometric and morphotectonic parameters in Upper Alaknanda river basin. Nat. Hazards 103, 3263–3301. https://doi.org/10.1007/s11069-020-04129-y

Papaioannou, G., Vasiliades, L., Loukas, A., 2014. Multi-criteria analysis framework for potential flood prone areas mapping. Water Resour. Manage. 29, 399–418. https://doi.org/10.1007/s11269-014-0817-6

Parveen, R., Kumar, U., Singh, V.K., 2012. Geomorphometric characterization of upper South Koel basin, Jharkhand: a remote sensing & GIS approach. J. Water Resource Prot. 4(12), 1042–1050. http://dx.doi.org/10.4236/jwarp.2012.412120

Patton, P.C., Baker, V.R., 1976. Morphometry and floods in small drainage basins subject to diverse hydro-geomorphic controls. Water Resour. Res. 12(5), 941–952. https://doi.org/10.1029/WR012i005p00941

Pei, T., Qin, C.Z., Zhu, A.X., Yang, L., Luo, M., Li, B., Zhou, C., 2010. Mapping soil organic matter using the topographic wetness index: a comparative study based on different flow-direction algorithms and kriging methods. Ecol. Indic. 10 (3), 610–619. https://doi.org/10.1016/j.ecolind.2009.10.005

Persichillo, M.G., Bordoni, M., Cavalli, M., Crema, S., Meisina, C., 2018. The role of human activities on sediment connectivity of shallow landslides. Catena 160, 261–274. https://doi.org/10.1016/j.catena.2017.09.025

Poeppl, R.E., Keesstra, S.D., Maroulis, J., 2017. A conceptual connectivity framework for understanding geomorphic change in human-impacted fluvial systems. Geomorphology 277, 237–250. https://doi.org/10.1016/j.geomorph.2016.07.033

Poeppl, R.E., Fryirs, K.A., Tunnicliffe, J., Brierley, G.J., 2020. Managing sediment (dis)connectivity in fluvial systems. Sci. Total Environ. 736, 139627. https://doi.org/10.1016/j.scitotenv.2020.139627

Pradhan, N.S., Das, P.J., Gupta, N., Shrestha, A.B., 2021. Sustainable management options for healthy rivers in South Asia: The Case of Brahmaputra. Sustainability 13(3), 1087. https://doi.org/10.3390/su13031087

Prasanna, V., Subere, J., Das, K.D., Govindarajan, S., Yasunari, T., 2014. Development of daily gridded rainfall dataset over the Ganga, Brahmaputra and Meghna river basins. Meteorol. Appl. 21, 278–293. https://doi.org/10.1002/met.1327

R Development Core Team, 2020. A language and environment for statistical computing. R foundation for statistical computing. https://www.R-project.org.

Rafaelli, S.G., Montgomery, D.R., Greenberg, H.M., 2001. A comparison of thematic mapping of erosional intensity to GIS-driven process models in an Andean drainage basin. J. Hydrol. 244, 33–42. https://doi.org/10.1016/S0022-1694(00)00419-4

Rajbanshi, J., Das, S., Patel, P., 2022. Planform changes and alterations of longitudinal connectivity caused by the 2019 flood event on the braided Brahmaputra River in Assam, India. Geomorphology 403, 108174. https://doi.org/10.1016/j.geomorph.2022.108174

Rai, P. K., Mishra, V. N., Mohan, K., 2017. A study of morphometric evaluation of the Son basin, India using geospatial approach. Remote Sens. Appl.: Soc. Environ. 7, 9–20. https://doi.org/10.1016/j.rsase.2017.05.001

Rahaman, M.M., Varis, O., 2009. Integrated water management of the Brahmaputra Basin: Perspectives and hope for regional development. Nat. Resour. Forum 33, 60–75. https://doi.org/10.1111/j.1477-8947.2009.01209.x

Rahman, M., Dustegir, M., Karim, R., Haque, A., Nicholls, R.J., Darby, S.E., Nakagawa, H., Hossain, M., Dunn, F.E., Akter, M., 2018. Recent sediment flux to the Ganges–Brahmaputra-Meghna delta system. Sci. Total Environ. 643, 1054–1064. https://doi.org/10.1016/j.scitotenv.2018.06.147

Rahmati, O., Samadi, M., Shahabi, H., Azareh, A., Rafiei-Sardooi, E., Alilou, H., Melesse, A.M., Pradhan, B., Chapi, K., Shirzadi, A., 2019. SWPT: An automated GIS-based tool for prioritization of sub-watersheds based on morphometric and topo-hydrological factors. Geosci. Front. 10(6), 2167–2175. https://doi.org/10.1016/j.gsf.2019.03.009

Rao, M.P., Cook, E.R., Cook, B.I., D'Arrigo, R.D., Palmer, J.G., Lall, U., Woodhouse, C.A., Buckley, B.M., Uriarte, M., Bishop, D.A., Jian, J., Webster, P.J., 2020. Seven centuries of reconstructed Brahmaputra River discharge demonstrate underestimated high discharge and flood hazard frequency. Nat. Commun. 11, 6017. https://doi.org/10.1038/s41467-020-19795-6

Rasul, G., 2015. Water for growth and development in the Ganges, Brahmaputra, and Meghna basins: an economic perspective. Int. J. River Basin Manage. 13(3), 387–400. https://doi.org/10.1080/15715124.2015.1012518

Ray, P.A., Yang, Y.C.E., Wi, S., Khalil, A., Chatikavanij, V., Brown, C., 2015. Room for improvement: Hydroclimatic challenges to poverty-reducing development of the Brahmaputra River basin. Environ. Sci. Policy 54, 64–80. https://doi.org/10.1016/j.envsci.2015.06.015

Rhoads, B., 2020. The Vertical Dimension of Rivers: Longitudinal Profiles, Profile Adjustments, and Step-Pool Morphology. In River Dynamics: Geomorphology to Support Management, Cambridge University Press, pp. 294–318. http://doi.org/10.1017/9781108164108.013

Rickenmann, D., Zimmermann, M., 1993. The 1987 debris flows in Switzerland: documentation and analysis. Geomorphology 8 (2–3), 175–189. https://doi.org/10.1016/0169-555X(93)90036-2

Richards, A., Parrish, R., Harris, N., Argles, T., Zhang, L., 2006. Correlation of lithotectonic units across the eastern Himalaya, Bhutan. Geology 34, 341–344. https://doi.org/10.1130/G22169.1

Różycka, M., Migoń, P., 2021. Morphometric properties of river basins as indicators of relative tectonic activity-Problems of data handling and interpretation. Geomorphology 389, 107807. https://doi.org/10.1016/j.geomorph.2021.107807

Roy, L., Das, S., 2021. GIS-based landform and LULC classifications in the Sub-Himalayan Kaljani Basin: Special reference to 2016 Flood. Egypt. J. Remote. Sens. Space Sci. 24(3), 755-767. https://doi.org/10.1016/j.ejrs.2021.06.005

Rudraiah, M., Govindaiah, S., Srinivas, V.S., 2008. Morphometry using remote sensing and GIS techniques in the sub basins of Kagna river basin, Gulburga district, Karnataka, India. J. Indian Soc. Remote Sens. 36, 351–360. https://doi.org/10.1007/s12524-008-0035-x

Saha, U.D., Bhattacharya, S., 2019. Reconstructing the channel shifting pattern of the Torsa River on the Himalayan Foreland Basin over the last 250 years. Bulletin of Geography, Physical Geography Series 16 (1), 99–114. https://doi.org/10.2478/bgeo-2019-0007

Saha, U.D., Bhattacharya, S., 2021. Channel avulsion in the Torsa River course and its response to topographic and hydrological controls on the Himalayan Foreland Basin. J Earth Syst. Sci.130, 184. https://doi.org/10.1007/s12040-021-01669-0

Sangireddy, H., Carothers, R.A., Stark, C.P., Passalacqua, P., 2016. Controls of climate, topography, vegetation, and lithology on drainage density extracted from high resolution topography data. J. Hydrol. 537, 271–282. https://doi.org/10.1016/j.jhydrol.2016.02.051

Sarker, M.H., Thorne, C.R., Aktar, M.N., Ferdous, M.R., 2014. Morpho-dynamics of the Brahmaputra-Jamuna River, Bangladesh. Geomorphology 215, 45–59. https://doi.org/10.1016/j.geomorph.2013.07.025

Sarma, J.N., 2004. An Overview of the Brahmaputra River System. In: Singh, V.P., Sharma, N., Ojha, C.S.P. (Eds.), The Brahmaputra Basin Water Resources. Water Science and Technology Library 47, 72–87. https://doi.org/10.1007/978-94-017-0540-0_5

Sarma, J.N., 2005. Fluvial process and morphology of the Brahmaputra River in Assam, India. Geomorphology 70, 226–256. https://doi.org/10.1016/j.geomorph.2005.02.007

Schumm, S.A., 1956. Evolution of drainage systems and slopes in badlands at Perth Amboy, New Jersey. Geol. Soc. Am. Bull. 67 (5), 597–646. https://doi.org/10.1130/0016-7606(1956)67[597:EODSAS]2.0.CO;2

Schwanghart, W., Scherler, D., 2017. Bumps in river profiles: Uncertainty assessment and smoothing using quantile regression techniques. Earth Surf. Dynam. 5(4), 821–839. https://doi.org/10.5194/esurf-5-821-2017

Sharma, S., Sarma, J.N., 2013. Drainage analysis in a part of the Brahmaputra Valley in Sivasagar District, Assam, India, to detect the role of nontectonic activity. J. Indian Soc. Remote Sens. 41(4), 895–904. https://doi.org/10.1007/s12524-013-0262-7

Sharma, A., 2010. Integrating terrain and vegetation indices for identifying potential soil erosion risk area. Geo-spat. Info. Sci. 13(3), 201–209. https://doi.org/10.1007/s11806-010-0342-6

Sharma, N., Sarkar, A., Akhter, P., Kumar, N., 2012. National Disaster Management Authority of India (NDMA) final report on study of Brahmaputra River erosion and its control. Conducted by Department of Water Resource Development and Management, India Institute of Technology, Roorkee. https://ndma.gov.in/sites/default/files/PDF/Technical%20Documents/NDMA%20Final%20Report%20Brahmaputra%20River.pdf (accessed on 25 June 2021)

Shi, X., Yang, Z., Dong, Y., Qu, H., Zhou, B., Cheng, B., 2020. Geomorphic indices and longitudinal profile of the Daba Shan, northeastern Sichuan Basin: Evidence for the late Cenozoic eastward growth of the Tibetan Plateau. Geomorphology 353, 107031. https://doi.org/10.1016/j.geomorph.2020.107031

Shrestha, M.S., Artan, G.A., Bajracharya, S.R., Sharma, R.R., 2008. Using satellite-based rainfall estimates for streamflow modelling: Bagmati Basin. J. Flood Risk Management 1, 89–99. https://doi.org/10.1111/j.1753-318X.2008.00011.x

Shukla, A.K., Ojha, C.S.P., Garg, R.D., 2014. Satellite based estimation and validation of monthly rainfall distribution over upper Ganga river basin. Int. Arch. Photogramm. Remote Sens. Spatial Inf. Sci. XL–8, 399–404. https://doi.org/10.5194/isprsarchives-XL-8-399-2014

Siddiqui, S., Chohan, S., Das, P.J., 2018. Reimagining Brahmaputra: Policy and Regulatory Aspects of Transboundary Water Governance; Oxfam: New Delhi, India.

Singh, S.K., 2007. Erosion and Weathering in the Brahmaputra River System. In: Gupta, A. (Eds.), Large Rivers: Geomorphology and Management. John Wiley & Sons, Ltd. pp. 373–393. https://doi.org/10.1002/9780470723722.ch18

Singh, S.K, France-Lanord, C., 2002. Tracing the distribution of erosion in the Brahmaputra watershed from isotopic compositions of stream sediments, Earth Planet. Sci. Lett. 202 (3–4), 645–662. https://doi.org/10.1016/S0012-821X(02)00822-1

Singh, V.P., Sharma, B., Shekhar, C., Ojha, P., 2004. The Brahmaputra Basin Water Resources. Kluwer Academic Publishers. Dordrecht, Boston.

Singh, M., Sinha, R., Tandon, S.K., 2021. Geomorphic connectivity and its application for understanding landscape complexities: a focus on the hydro-geomorphic systems of India. Earth Surf. Process. Landforms 46, 110–130. https://doi.org/10.1002/esp.4945

Sinha, R., Friend, P.F., 1994. River systems and their sediment flux, Indo-Gangetic plains, northern Bihar, India. Sedimentology 41, 825–845. https://doi.org/10.1111/j.1365-3091.1994.tb01426.x

Sinha, R., Jain, V., Prasad Babu, G., Ghosh, S., 2005. Geomorphic characterization and diversity of the rivers of the Gangetic plains. Geomorphology 70, 207–225. https://doi.org/10.1016/j.geomorph.2005.02.006

Sinha, R., Jain, V., Tandon, S.K., 2013. River Systems and River Science in India: Major Drivers and Challenges. In: Sinha, R., Ravindra, R. (Eds.), Earth System Processes and Disaster Management. Society of Earth Scientists Series. Springer, Berlin, Heidelberg, pp. 67–90. https://doi.org/10.1007/978-3-642-28845-6_6

Sinha, R., Ravindra, R., 2013. Earth System Processes and Disaster Management. Society of Earth Scientists Series. Springer Berlin, Heidelberg. https://doi.org/10.1007/978-3-642-28845-6

Smith, P.N.H., 1997. Hydrologic data development system. Transp. Res. Rec. 1599 (1), 118–127. https://doi.org/10.3141/1599-15

Sørensen, R., Zinko, U., Seibert, J., 2006. On the calculation of the topographic wetness index: evaluation of different methods based on field observations. Hydrol. Earth Syst. Sci. 10, 101–112. https://doi.org/10.5194/hess-10-101-2006

Sørensen, R., Seibert, J., 2007. Effects of DEM resolution on the calculation of topographical indices: TWI and its components. J. Hydrol. 347(1–2), 79–89. https://doi.org/10.1016/j.jhydrol.2007.09.001

Sreedevi, P.D., Owais, S., Khan, H.H., Ahmed, S., 2009. Morphometric analysis of a Watershed of south India using SRTM data and GIS. J Geol. Soc. India 73, 543–552. https://doi.org/10.1007/s12594-009-0038-4

Strahler, A.N., 1952. Hypsometric (area-altitude) analysis of erosional topography. Geol. Soc. Am. Bull. 63(11), 1117–1142. https://doi.org/10.1130/0016-7606(1952)63[1117:HAAOET]2.0.CO;2

Strahler, A.N., 1964. Quantitative Geomorphology of Drainage Basins and Channel Networks. In: Chow, V., (Eds.), Handbook of Applied Hydrology, New York, McGrawHill, pp. 439–476.

Stark, C.P., Stark, G.J., 2001. A channelization model of landscape evolution. Am. J. Sci. 301 (4–5), 486–512. https://doi.org/10.2475/ajs.301.4-5.486

Subramanian, V., Ramanathan, A.L., 1996. Nature of Sediment Load in the Ganges–Brahmaputra River Systems in India. In: Milliman, J.D., Haq, B.U. (Eds.), Sea-Level Rise and Coastal Subsidence. Coastal Systems and Continental Margins, vol 2. Springer, Dordrecht, pp. 151–168. https://doi.org/10.1007/978-94-015-8719-8_8

Sujatha, E.R., Selvakumar, R., Rajasimman, U.A.B., 2014. Watershed prioritization of Palar sub-watershed based on the morphometric and land use analysis. J. Mt. Sci. 11(4), 906–916. https://doi.org/10.1007/s11629-012-2628-7

Swarnkar, S., Sinha, R., Tripathi, S., 2020. Morphometric diversity of supply-limited and transport-limited river systems in the Himalayan foreland. Geomorphology 348, 106882. https://doi.org/10.1016/j.geomorph.2019.106882

Takagi, T., Oguchi, T., Matsumoto, J., Grossma, M.J., Sarker, M.H., Matin, M.A., 2007. Channel braiding and stability of the Brahmaputra River, Bangladesh, since 1967: GIS and remote sensing analyses. Geomorphology 85, 294–305. https://doi.org/10.1016/j.geomorph.2006.03.028

Takahashi, T., 1981. Estimation of potential debris flows and their hazardous zones; soft countermeasures for a disaster. J. Nat. Disaster Sci. 3, 57–89. http://dl.ndl.go.jp/info:ndljp/pid/10752573

Tarboton, D., 1997. A new method for the determination of flow directions and upslope areas in grid digital elevation models. Water Resour. Res. 33(1), 309–319. https://doi.org/10.1029/96WR03137

Tarek, M.H., Hassan, A., Bhattacharjee, J., Choudhury, S.H., Badruzzaman, A.B.M., 2017. Assessment of TRMM data for precipitation measurement in Bangladesh. Meteorol. Appl. 24, 349–359. https://doi.org/10.1002/met.1633

Tarolli, P., Sofia, G., 2016. Human topographic signatures and derived geomorphic processes across landscapes. Geomorphology 255, 140–161. https://doi.org/10.1016/j.geomorph.2015.12.007

Tran, T., Nguyen, B.Q., Vo, N.D., Le, M., Nguyen, Q., Lakshmi, V., Bolten, J.D., 2023. Quantification of global Digital Elevation Model (DEM)–A case study of the newly released NASADEM for a river basin in Central Vietnam. J. Hydrol.: Regional Studies 45, 101282. https://doi.org/10.1016/j.ejrh.2022.101282

Tropical Rainfall Measuring Mission (TRMM), 2011. TRMM (TMPA/3B43) Rainfall Estimate L3 1 month 0.25 degree x 0.25 degree V7, Greenbelt, MD, Goddard Earth Sciences Data and Information Services Center (GES DISC). http://doi.org/10.5067/TRMM/TMPA/MONTH/7 (Accessed on 20 March 2021).

Tucker, G.E., Bras, R.L., 1998. Hillslope processes, drainage density and landscape morphology. Water Resour. Res. 34, 2751–2764. https://doi.org/10.1029/98WR01474

Turley, M., Hassan, M.A., Slaymaker, O., 2021. Quantifying sediment connectivity: Moving toward a holistic assessment through a mixed methods approach. Earth Surf. Process. Landforms. 46(12), 2501–2519. https://doi.org/10.1002/esp.5191

Turnbull, L., Wainwright, J., Brazier, R.E., 2008. A conceptual framework for understanding semi-arid land degradation: eco-hydrological interactions across multiple-space and time scales. Ecohydrol. 1, 23–34. https://doi.org/10.1002/eco.4

Uuemaa, E., Ahi, S., Montibeller, B., Muru, M., Kmoch, A., 2020. Vertical accuracy of freely available global digital elevation models (ASTER, AW3D30, MERIT, TanDEM-X, SRTM, and NASADEM). Remote Sens. 12 (21), 3482. https://doi.org/10.3390/rs12213482

Umitsu, M., 1987. Late quaternary sedimentary environment and landform evolution in the Bengal lowland. Geogr. Rev. Jpn. (ser B) 60 (2), 164–178. https://doi.org/10.4157/grj1984b.60.164

Van Dine, D., 1996. Debris flow control structures for forest engineering. Research Branch, Ministry of Forests, Victoria. BC. Working Paper 08/1996. https://www.for.gov.bc.ca/hfd/pubs/docs/wp/wp22.pdf (accessed on 10 May 2021)

Vijith, H., Dodge-Wan, D., 2019. Modelling terrain erosion susceptibility of logged and regenerated forested region in northern Borneo through the Analytical Hierarchy Process (AHP) and GIS techniques. Geoenvironmental Disasters 6, 8. https://doi.org/10.1186/s40677-019-0124-x

Wasson, R.A., 2003. A sediment budget for the Ganga–Brahmaputra catchment. Curr. Sci. 84, 1041–1047. https://www.jstor.org/stable/24107666

Whipple, K.X., Tucker, G.E., 1999. Dynamics of the stream-power river incision model: implications for height limits of mountain ranges, landscape response timescales, and research needs. J. Geophys. Res. 104(B8), 17661–17674. https://doi.org/10.1029/1999JB900120

Winchell, M.F., Jackson, S.H., Wadley, A.M., Srinivasan, R., 2008. Extension and validation of a geographic information system-based method for calculating the revised universal soil loss equation length-slop factor for erosion risk assessments in large watersheds. J. Soil Water Conserv. 63(3), 105-111. https://doi.org/10.2489/jswc.63.3.105

Wischmeier, W.H., Smith, D.D., 1978. Predicting rainfall erosion losses: a guide to conservation planning. US Department of Agriculture Handbook, No. 537, Washington DC. https://naldc.nal.usda.gov/download/CAT79706928/PDF (accessed on 20 May 2021)

Weiss, A.D., 2001. Topographic position and landform analysis. In: Poster presentation, ESRI users conferences, San Diego, CA. http://www.jennessent.com/downloads/tpi-poster-tnc_18x22.pdf. (accessed on October 2021)

Wohl, E., Merritt, D.M., 2008. Reach-scale channel geometry of mountain streams. Geomorphology 93(3–4), 168–185. https://doi.org/10.1016/j.geomorph.2007.02.014

Wohl, E., Brierley, G., Cadol, D., Coulthard, T.J., Covino, T., Fryirs, K.A., Grant, G., Hilton, R.G., Lane, S.N., Magilligan, F.J., Meitzen, K.M., Passalacqua, P., Poeppl, R.E., Rathburn, S.L., Sklar, L.S., 2019. Connectivity as an emergent property of geomorphic systems. Earth Surf. Process. Landforms 44(1), 4–26. https://doi.org/10.1002/esp.4434

World Bank Group, 2015. Toward Efficient and Sustainable River Basin Operational Services in Indonesia. World Bank, Washington, DC. https://openknowledge.worldbank.org/handle/10986/23241 (accessed on May 2021).

White, S.M., Apitz, S.E., 2008. Conceptual and strategic frameworks for sediment management at the river basin scale. In: Owens, P. N. (Eds.), Sediment Management of Sediment Resources: Sediment Management at the River Basin Scale, Elsevier BV, pp. 31–53. https://doi.org/10.1016/s1872-1990(08)80004-9

Whipple, K.X., Tucker, G.E., 1999. Dynamics of the stream-power river incision model: implications for height limits of mountain ranges, landscape response timescales, and research needs. J. Geophys. Res. 104, 17661–17674. https://doi.org/10.1029/1999JB900120

Xiao, H., Liu, G., Liu, P., Zheng, F., Zhang, J., Hu, F., 2017. Sediment transport capacity of concentrated flows on steep loessial slope with erodible beds. Sci. Rep. 7, 2350. https://doi.org/10.1038/s41598-017-02565-8

Xie, C., Cui, B., Xie, T., Yu, S., Liu, Z., Chen, C., Shao, X., 2020. Hydrological connectivity dynamics of tidal flat systems impacted by severe reclamation in the Yellow River Delta. Sci. Total Environ. 739, 139860. https://doi.org/10.1016/j.scitotenv.2020.139860

Yasuda, Y., Aich, D., Hill, D., Huntjens, P., Swain, A., 2017. Transboundary Water Cooperation over the Brahmaputra River: Legal Political Economy Analysis of Current and Future Potential Cooperation. The Hague Institute for Global Justice. https://siwi.org/wp-content/uploads/2018/01/brahmaputra-basin-report-final_design.pdf (accessed on 10 March 2022)

Yong, B., Chen, B., Gourley, J.J., Ren, L., Hong, Y., Chen, X., Wang, W., Chen, S., Gong, L., 2014. Inter comparison of the Version-6 and Version-7 TMPA precipitation products over high and low latitudes basins with independent gauge networks: is the newer version better in both real-time and post-real-time analysis for water resources and hydrologic extremes? J. Hydrol. 508, 77–87. https://doi.org/10.1016/j.jhydrol.2013.10.050

Zanandrea, F., Michel, G.P., Kobiyama, M., Cardozo, G.L., 2019. Evaluation of different DTMs in sediment connectivity determination in the Mascarada River Watershed, southern Brazil. Geomorphology 332, 80–87. https://doi.org/10.1016/j.geomorph.2019.02.005

Zanandrea, F., Michel, G. P., Kobiyama, M., Censi, G., Abatti, B. H. 2021. Spatial-temporal assessment of water and sediment connectivity through a modified connectivity index in a subtropical mountainous catchment. Catena, 204, 105380. https://doi.org/10.1016/j.catena.2021.105380

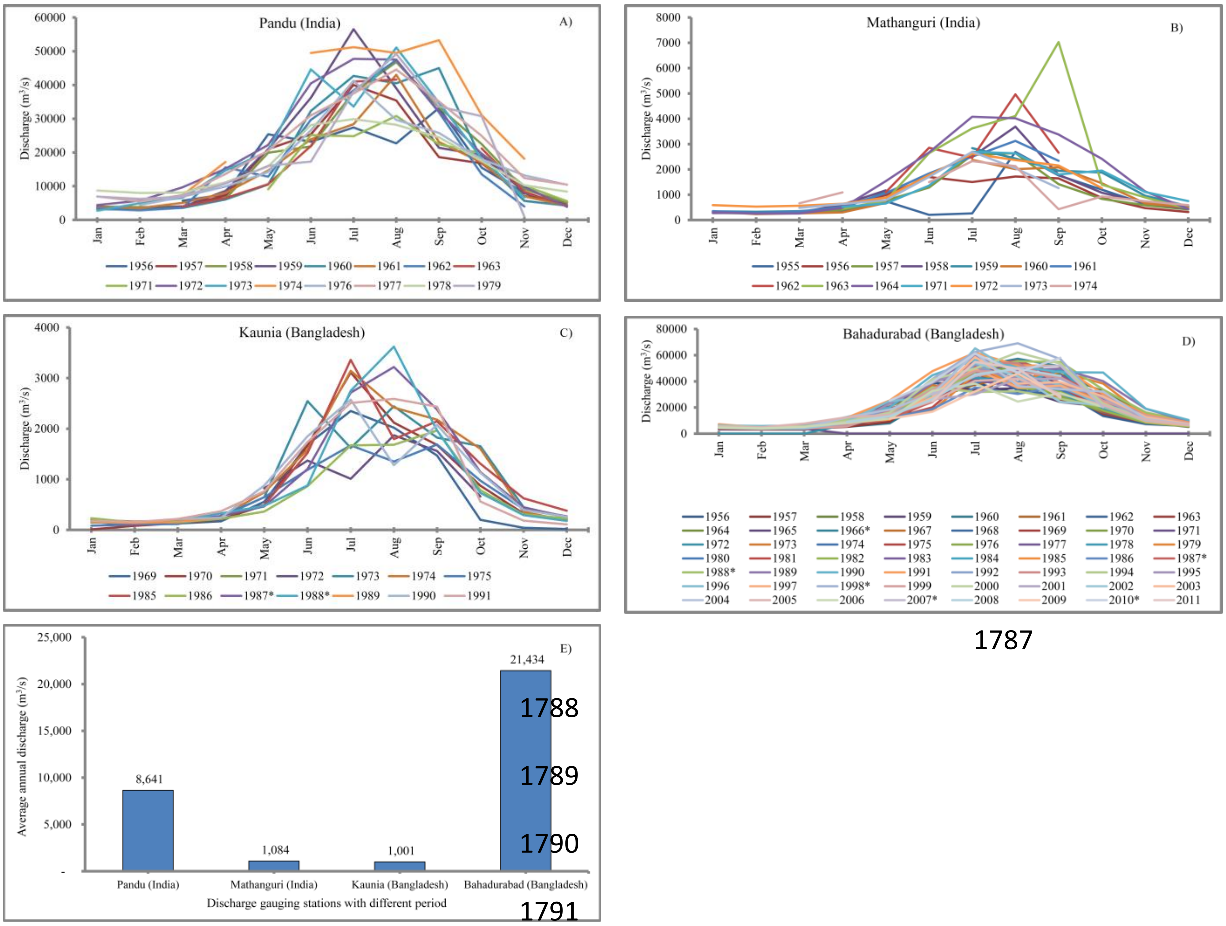

Supplementary Fig. S1. Monthly discharge hydrographs from different gauging stations along the study area; A. Pandu (India) (1956-1963, 1971-1979); B) Mathanguri (India) (1955-1964, 1971-1974); C) Kaunia (Bangladesh) (1969-1975, 1985-1991); D) Bahadurabad (Bangladesh) (1956-2011); E) Average annual discharge at different gauging stations. * denotes the major flood occurrence.

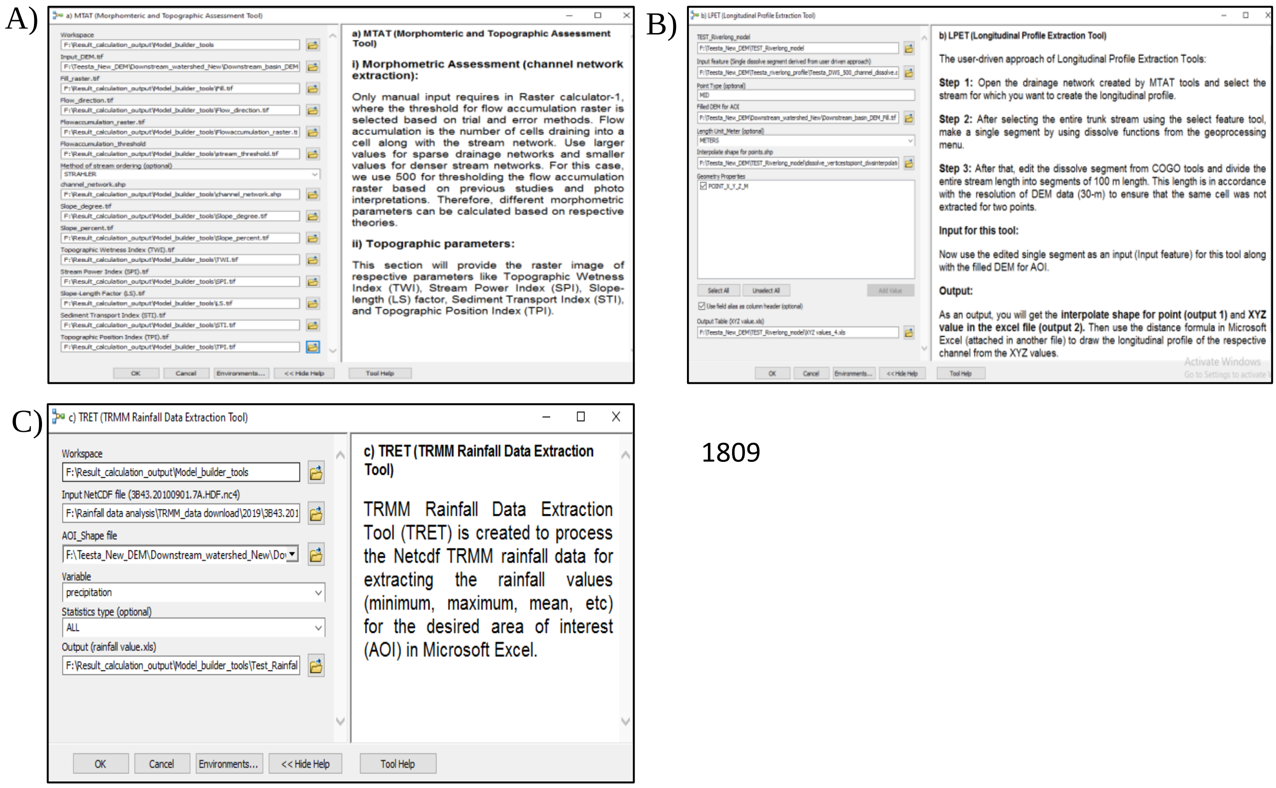

Supplementary Fig. S2. Workflow of deriving morphometric parameters converted to Semi-automated Morphometric Assessment Tools (SMAT); A) Morphometric and Topographic Assessment Tool (MTAT), B) Longitudinal Profile Extraction Tool (LPET), and C) TRMM Rainfall Data Extraction Tool (TRET).

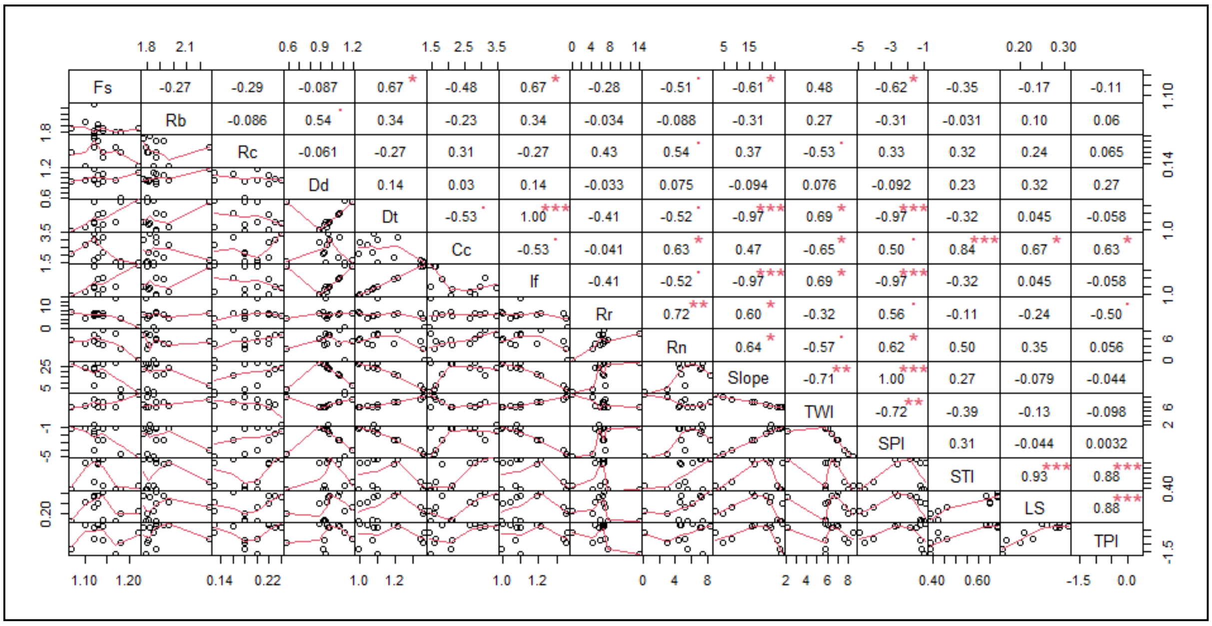

Supplementary Fig. S3. The correlation matrix represents the relationships and relative importance of morphometric and topographic indices (abbreviations are according to Table 3). The right half shows the Pearson correlation matrix with the significance level (***P<0.001; **P<0.01, *P<0.05). The left half is the data distribution and bivariate scatter plot with fitted lines.

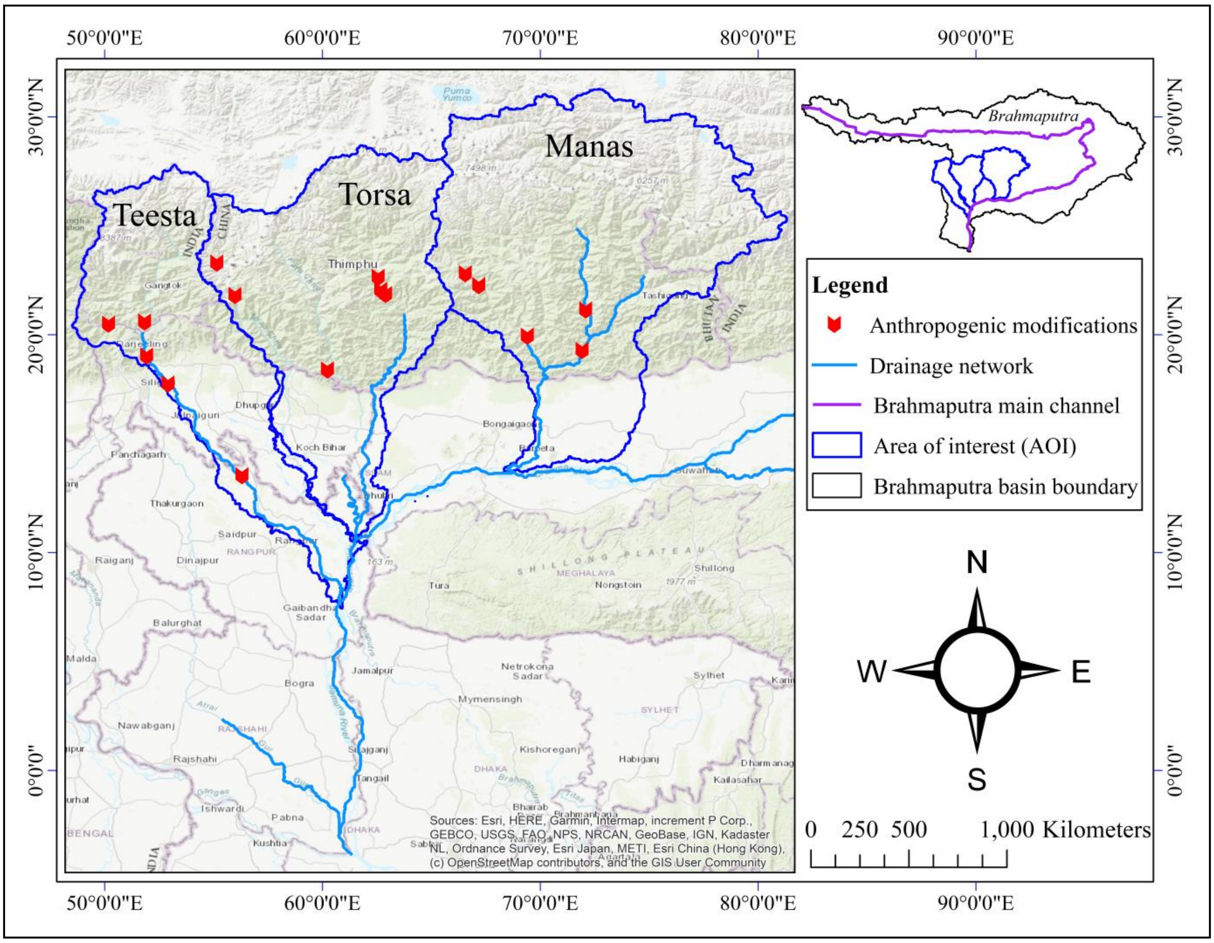

Supplementary Fig. S4. The spatial distribution of anthropogenic inferences (dams, barrages, hydroelectric plants, channel diversion, and hydro-engineering structures) along Brahmaputra basins (Teesta, Torsa, and Manas) is shown with background topography as an example. The enlisted (16) anthropogenic modifications are the i) Teesta low DAM-III, ii) Rammam hydroelectric project-III, iii) Teesta low DAM- IV project, iv) Gazoldoba barrage & diversion at Teesta (India), v) Teesta barrage & diversion (Bangladesh), vi) Punatsangchhu-I hydroelectric project, vii) Punatsangchhu-II hydroelectric project, viii) Basochhu hydropower project, ix) Kurichu hydroelectric project, x) Mandechchhu hydroelectric project, xi) Tangsibji micro hydropower plant, and xii-xvi) Hydro-engineering structures. The location and name of the anthropogenic modifications are based on google earth satellite imagery.

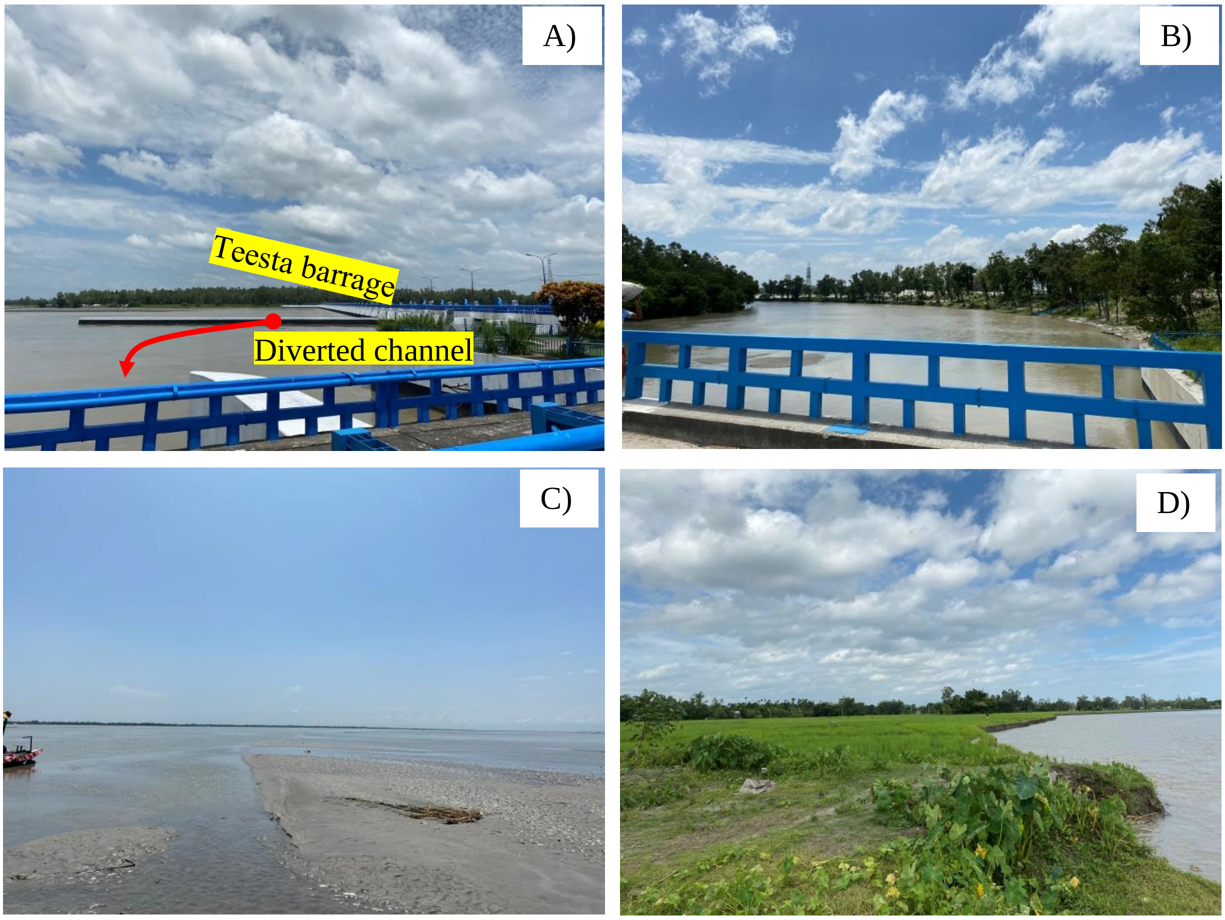

Supplementary Fig. S5. A) Teesta barrage in Bangladesh, B) diversion of channel from the barrage for irrigation, C) deposition within the channel, and D) erosion along the bank.

Supplementary Table S1. Results of Generalized linear mixed models (GLMMs) testing the effects of morphometric and topographic factors on connectivity (IC). The models were summarized as A) multivariate, B) univariate, and C) Null model in the table.

Explanatory variables	Log-likelihood	Akaike information criterion (AIC)	P value
A) Multivariate model			
SPI× R_n×F_s× D_d×R_b	1.89	18.20	<0.001***
B) Univariate models			
SPI	-8.60	27.20	<0.001***
R_n	-9.02	28.00	<0.001***
F_s	-7.90	29.50	0.022 *
D_d	-11.91	33.80	<0.001***
R_b	-11.88	33.80	0.0087 **
C) Null model	-11.91	31.80	

Note: When there are multiple explanatory variables that often have correlations with each other, this can lead to a distortion of the effects of the explanatory variables on the response variables due to collinearities with redundant effects. For this reason, explanatory variables without strong correlations (correlation coefficient > 0.7; $p < 0.05$) to others were selected to be included in GLMMs to avoid multicollinearity (Dormann et al., 2013). The GLMMs were constructed by considering stream power index (SPI), ruggedness number (R_n), stream frequency (F_s), drainage density (D_d), and bifurcation ratio (R_b) as main factors, IC as a response variable, and sub-basin nested within the basin as a random variable. Multivariate and univariate models denote the interaction and univariate effects on response variable, respectively. All models were compared separately with null models.